Preserving non-negative porosity values in a bi-phase elasto-plastic material under Terzaghi's effective stress principle.

Giuliano Pretti[a], William M. Coombs[a,*], Charles E. Augarde[a], Marc Marchena Puigvert[b], José Antonio Reyna Gutiérrez[b]

[a] *Department of Engineering, Durham University*
Science Site, South Road, Durham, DH1 3LE, UK.
[b] *Ørsted, Gentofte, Denmark*

Abstract

Poromechanics is a well-established field of continuum mechanics which seeks to model materials with multiple phases, usually a stiff solid phase and fluid phases of liquids or gases. Applications are widespread particularly in geomechanics where Terzaghi's effective stress is widely used to solve engineering soil mechanics problems. This approach assumes that the solid phase is incompressible, an assumption that leads to many advantages and simplifications without major loss of fidelity to the real world. Under the assumption of finite (as opposed to infinitesimal) strains, the poromechanics of two- or bi-phase materials gains complexity and while the compressible solid phase case has received attention from researchers, the incompressible case has received less. For the finite strain - incompressible solid phase case there is a fundamental issue with standard material models, in that for some loadings solid skeleton mass conservation is violated and negative Eulerian porosities are predicted. While, to the authors' best knowledge, acknowledgement of this essential problem has been disregarded in the literature, an elegant solution is presented here, where the constraint on Eulerian porosity can be incorporated into the free energy function for a material. The formulation is explained in detail, soundly grounded in the laws of thermodynamics and validated on a number of illustrative examples.

*Corresponding author: w.m.coombs@durham.ac.uk

1. Introduction

Poromechanics is the branch of mechanics describing the behaviour of porous media significantly influenced by the fluids which saturate the pore space. Various materials can be ascribed to this category, whose engineering applications range enormously: for instance environmental engineering, mining and petroleum engineering, geotechnical and seismic engineering, industrial engineering, bioengineering and biomechanics; for examples see [1–6].

If considering a single fluid filling the pore volume (a bi-phase material), the theoretical foundations for describing its mechanical behaviour were laid down in a series of seminal works by Biot [7–9]. However, the first investigations of such materials are even earlier (see, in this regard, de Boer and Ehlers [10]). The extension of Biot's theory to finite strains has since been pursued in numerous publications (see, for instance, MacMinn *et al.* [11] for a detailed comparison between small and finite strain poroelasticity). The interested reader can refer to the thorough bibliographies presented in Selvadurai and Surovov [12] and Zhang [13].

As far as the hydro-mechanical behaviour of a bi-phase material is concerned, there are essentially three ways in which there can be volume change (Figure 1). Two of these relate to the individual constituents, i.e. the compressibility of the individual phases (solid and liquid), while the third concerns the boundary conditions imposed on the fluid phase, i.e., the so-called drained or undrained conditions. Hence, when dealing with numerical analyses, while boundary conditions are associated with the problem under consideration, the choice of the compliance of single constituents is informed by the physics of the problem and the materials modelled. As emphasised by Nedjar's work [14, 15], these choices, especially when made in conjunction with the assumption of finite strains, must also be combined with the physical condition that the Eulerian porosity n (defined as the ratio of the current volume occupied by the fluid part over the total current volume) is physically constrained in the range between 0 and 1. In particular, Nedjar [14, 15] analysed how in-

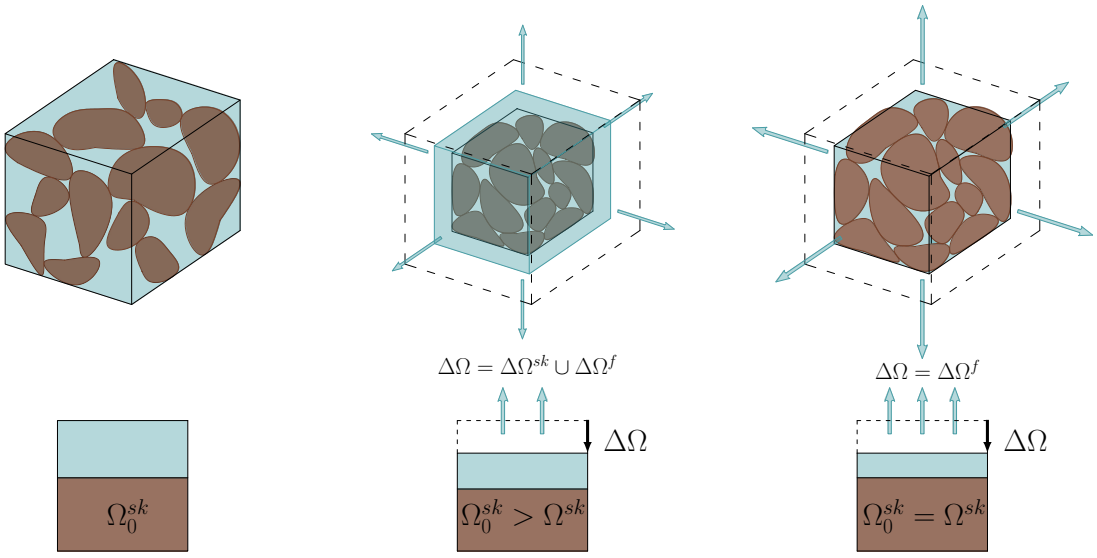

(a) Initial sample

(b) Option 1: Compressible solid matrix

(c) Option 2: Incompressible solid matrix

Figure 1: Comparison of drained volumetric compression in three dimensions with grains (top row) and idealised bi-dimensional boxes (bottom row). From the initial configuration (a), the same drained volumetric compression is applied to a compressible solid matrix sample (b) and to an incompressible solid matrix sample (c).

corporating bounded Eulerian porosity values has consequences when both solid and fluid phases are compressible (the case illustrated in Figure 1b). While it is widely recognised (see Bennethum [16]) that considering the solid phase (henceforth also referred to as the solid matrix or solid skeleton) as incompressible considerably simplifies the relationship between the phases, the consequences of such an assumption (especially in light of the constrained values of Eulerian porosity) have not been discussed in the literature and this is the main topic of this paper. Here we show how the hypothesis of incompressibility of the solid phase[1] (considered in Figure 1c for the case of drained volumetric compression) leads to a violation of the skeleton mass conservation and unphysical negative Eulerian

[1]It must be highlighted that this work differs from the model proposed by Bernaud *et al.* [17], who investigated the consequences of the plastic incompressibility for a porous material. The hypothesis being considered here is the incompressibility of the entire solid phase, regardless of its decomposition into an elastic and plastic part.

porosities when standard finite strain models are used. A new model, developed from first principles of thermodynamics is developed and compared to previous work for the case of a compressible solid matrix. Within the finite strain theory, in the case of elastic strains, the model meets the principles of hyper-elasticity, and, in the elasto-plastic case, those of hyper-plasticity.

The outline of the manuscript is as follows: Section 2 introduces the founding assumptions of this work, comparing the thermodynamics of compressible and incompressible solid materials. Section 3 proposes a free energy function of the solid skeleton by modifying a Hencky material (originally proposed in [18]) as well as detailing its implementation for elastic and elasto-plastic materials. Section 4 shows by means of numerical examples how this new free energy function is required in constitutive models for routine geotechnical problems in elasticity and elasto-plasticity, highlighting the unsuitability of the original Hencky material for these applications. Conclusions and future work are outlined in Section 5. It is worth noticing that there are two ways to read this manuscript: one is to follow the outlined course of the paper throughout the sections; the other, particularly helpful for more implementation-oriented readers, consists of reading Section 3 and Appendix A, after having familiarised with the nomenclature at page 5.

2. Thermodynamic framework of bi-phase materials

Finite strain theory of poromechanics is widely established (see, for instance, Coussy [19], or Lewis and Schrefler [20]) using the nomenclature included here to characterise the different quantities considered. The assumed hypotheses which constitute the bases of the whole work are summarised below:

- the fully saturated porous material is treated as superimposition of two continua, the solid skeleton and the interstitial fluid, with non-occluded pore space. The presence of a double porosity network (see Coussy [19]) is excluded;
- thermal effects are neglected;

Nomenclature

$\dot{\bullet}$, $\ddot{\bullet}$	material (first and second) time derivative	$\boldsymbol{\epsilon}$	$\coloneqq \frac{1}{2}\ln(\boldsymbol{b})$, logarithmic strain tensor
$(\bullet)^T$	transpose of $(\bullet)$	ϵ_v	$\coloneqq \boldsymbol{\epsilon} : \boldsymbol{I}^{(2)}$, volumetric part of the logarithmic strain tensor
sym $(\bullet)$	$\coloneqq 1/2\left((\bullet)+(\bullet)^T\right)$		
$\boldsymbol{I}^{(2)}$	second-order identity tensor	$\boldsymbol{l}$	$\coloneqq \dot{\boldsymbol{F}}\boldsymbol{F}^{-1}$, velocity gradient
$:$	double contraction of tensors	$\boldsymbol{d}$	$\coloneqq \text{sym}(\boldsymbol{l})$, stretching tensor
$\otimes$	tensor product of tensors or vectors	$\boldsymbol{u}$	$\coloneqq \boldsymbol{x} - \boldsymbol{X}^{sk}$, solid displacement
$(\bullet)^f$	quantity related to the fluid phase	$\boldsymbol{\alpha}$	set of internal variables
$(\bullet)^{sk}$	quantity related to the solid skeleton	$\boldsymbol{\tau}$	Kirchhoff stress tensor
$(\bullet)_0$	quantity related to the initial configuration	p^f	fluid pressure (Cauchy measure of stress)
$\boldsymbol{X}^{sk}$	original position of the solid phase	ρ^f	intrinsic fluid density
$\boldsymbol{x}$	current position shared by the two phases	n	Eulerian porosity
$\boldsymbol{F}$	$\coloneqq \frac{\partial \boldsymbol{\varphi}^{\boldsymbol{sk}}(\boldsymbol{X}^{sk},t)}{\partial \boldsymbol{X}^{sk}}$, solid deformation gradient	ϕ	$\coloneqq Jn$, Lagrangian porosity
		m^f	$\coloneqq \rho^f\phi$, fluid mass content
J	$\coloneqq \det \boldsymbol{F}$, Jacobian	$\boldsymbol{q}^f$	$\coloneqq n\rho^f\left(\dot{\boldsymbol{x}}^f - \dot{\boldsymbol{x}}^s\right)$, fluid flux
$\boldsymbol{C}$	$\coloneqq \boldsymbol{F}^T\boldsymbol{F}$, right Cauchy-Green strain tensor	Ψ	free (Helmholtz) energy density per unit reference configuration
$\boldsymbol{b}$	$\coloneqq \boldsymbol{F}\boldsymbol{F}^T$, left Cauchy-Green strain tensor	$\boldsymbol{f}$	body acceleration vector

- the framework is cast within the finite strain theory, where $\boldsymbol{x}$ indicates the current position shared by the two constituents. The original position of the solid phase is indicated by $\boldsymbol{X}^{sk}$. The fluid phase's original position is not used throughout this work, and, as such, its notation is not introduced. Therefore, the deformation gradient and all the kinematical and statical quantities based on its definition are relative to the solid phase. For the sake of notation, the superscript is dropped from

these quantities. Elasto-plasticity is treated via the multiplicative decomposition of the elasto-plastic deformation gradient (firstly proposed by Kröner [21], Lee [22] and Mandel [23]). The effects of viscosity, either visco-elastic or visco-plastic, are not considered;

- there is no mass exchange between solid and fluid phases, i.e., mass conservation for the solid and fluid phases can be written separately;

- the considered continuum is *isotropic*;

Given the above assumptions, the strong (local) form of the Clausius-Planck inequality[2] for a porous saturated medium per unit current mixture volume is as follows

$$\underbrace{\frac{1}{J}\left(\boldsymbol{\tau} : \boldsymbol{d} + \dot{m}^f \mu^f - \dot{\Psi}\right)}_{:=\mathcal{D}^{sk}} \underbrace{- \left(\frac{1}{\rho^f}\frac{\partial p^f}{\partial \boldsymbol{x}} - \left(\boldsymbol{f} - \ddot{\boldsymbol{u}}^f\right)\right) \cdot \boldsymbol{q}^f}_{:=\mathcal{D}^f} \geq 0. \tag{1}$$

Focusing on $\mathcal{D}^f$, i.e., the fluid dissipation per unit reference volume, a constitutive relationship is necessary to describe how the fluid flux vector $\boldsymbol{q}^f$ relates to the gradient of pressure and the relative inertia components. For small Reynolds numbers (see, for instance, Sun *et al.* [26]), this relationship is linear and it is expressed by the *Darcy–Weisbach* formula, i.e.,

$$\boldsymbol{q}^f = -\rho^f \, k \left(\frac{\partial \, p^f}{\partial \boldsymbol{x}} - \rho^f \left(\boldsymbol{f} - \ddot{\boldsymbol{u}}^f\right)\right), \tag{2}$$

where the hypothesis of isotropic permeability is expressed by the simplification for the mobility tensor into $k_{ij} = k\,\delta_{ij}$. Replacing the unique inequality expressed by (1) with multiple inequalities (i.e., $\mathcal{D}^{sk} \geq 0$ and $\mathcal{D}^f \geq 0$) is a standard procedure (see, for instance,

[2] Bennett *et al.* [24] have shown the importance of an Eshelby-like stress tensor in the context of elasto-plasticity: this is the only stress tensor which satisfies the second law of thermodynamics and maintains the intermediate configuration as a stress-free state. However, since the Kirchhoff stress tensor does not violate the second law of thermodynamics, as stated in (1), (while it does not lead to intermediate stress-free configuration), this work continues (see, for instance, de Souza Neto *et al.* [25]) to traditionally consider the Kirchhoff stress tensor as an adequate measure to include plasticity.

Coussy [19]) justified by the different physical natures underlying the two diverse dissipation mechanisms. Owing to this observation and to Eq. (2), the dissipation denoted as $\mathcal{D}^f$ is always greater than or equal to zero.

According to the hypothesis of the mixture theory (see, in this regard, Bowen [27]), the total free energy functions Ψ can be expressed as a sum of their solid skeleton and their fluid constituent, i.e.,

$$\Psi = \Psi^{sk} + m^f \, \psi^f, \tag{3}$$

with ψ^f being the fluid-specific (per unit mass) free energy. It is also useful to express the fluid-specific free energy via other state variables, such as the fluid-specific enthalpy μ^f, the pressure p^f,and the current fluid density ρ^f, giving

$$\psi^f = \mu^f - \frac{p^f}{\rho^f}. \tag{4}$$

Using the above equations, $J\,\mathcal{D}^{sk}$ can be re-written as

$$J\,\mathcal{D}^{sk} = \boldsymbol{\tau} : \boldsymbol{d} + p^f \, \dot{\phi} - \dot{\Psi}^{sk} - \rho^f \, \phi \left(\dot{\mu}^f - \frac{\dot{p}^f}{\rho^f} \right) \geq 0. \tag{5}$$

The last term of the above inequality does not contribute to the dissipation if some additive hypotheses on the nature of the fluid are introduced[3]. In particular, by neglecting thermal effects and viscosity, the following two options can be considered: the fluid can be either *barotropic* (see, for instance, Armero [28]), i.e.,

$$\frac{\partial \mu^f}{\partial p^f} = \frac{1}{\rho^f \left(p^f \right)}, \tag{6}$$

[3]Introducing the hypothesis of barotropic or incompressible fluid is, by all means, a constitutive relationship. From a rigorous perspective, this step should be carried out via the *Coleman-Noll* procedure, described in Sections 2.1 and 2.2. However, as the focus of this work is on the part relative to the free energy function of the solid skeleton Ψ^{sk}, this hypothesis is implemented at this stage to simplify the calculations and highlight only the parts of interest for the current work. The same idea can be applied to the introduction of the Darcy–Weisbach (2) formula, as also this is a constitutive relationship.

or *incompressible* (see, for instance, Gajo [29]), i.e.,

$$\frac{\partial \mu^f}{\partial p^f} = \frac{1}{\rho_0^f}. \tag{7}$$

In the numerical examples presented in Section 4, the fluid part is considered as barotropic. However, regardless of the choice between barotropic or incompressible fluid constituent (or others available in the literature), the hypothesis on the fluid constituent relationship simplifies (5) to

$$J\,\mathcal{D}^{sk} = \boldsymbol{\tau} : \boldsymbol{d} + p^f\,\dot{\phi} - \dot{\Psi}^{sk} \geq 0. \tag{8}$$

So far, no assumption on the volumetric compressibility of the solid skeleton part has been introduced, which, as predictable, affects the way Ψ^{sk} describes the solid matrix behaviour. In particular, Section 2.1 considers the broader hypothesis of solid skeleton compliance, while incompressibility is assumed Section 2.2, laying the thermodynamical foundations for the novel constitutive relationship.

2.1. Thermodynamics for compressible solid matrix

Focusing only on the solid skeleton part of dissipation, it is straightforward to think the free energy of the solid skeleton as a function of the (external) variables explicitly appearing as rate quantities in (8). Furthermore, the dependency of this free energy function on a set of other internal variables (denoted as $\boldsymbol{\alpha}$) is introduced to take further dissipative mechanisms into account. Owing to the above considerations, Ψ^{sk} can be expressed as

$$\Psi^{sk} = \hat{\Psi}^{sk}\left(\boldsymbol{F}, \phi, \boldsymbol{\alpha}\right). \tag{9}$$

As objectivity of the free energy function is required (see, for instance, Simo [30]), the above dependency of the free energy function on the deformation gradient can be expressed via

the *right Cauchy-Green* strain tensor $\boldsymbol{C}$, i.e.,

$$\Psi^{sk} = \hat{\Psi}^{sk}\left(\boldsymbol{C}(\boldsymbol{F}), \phi, \boldsymbol{\alpha}\right), \tag{10}$$

where the reader is invited to overlook the slight abuse of notation $\hat{\Psi}^{sk}$, which is repeated throughout this work several times. Furthermore, considering the multiplicative decomposition of the deformation gradient into an elastic and a plastic part ($\boldsymbol{F} = \boldsymbol{F}^e\,\boldsymbol{F}^p$), the free energy function usually becomes dependent only on the elastic part of the deformation gradient $\boldsymbol{F}^e$ via the elastic right Cauchy-Green strain $\boldsymbol{C}^e\,(\boldsymbol{F}^e)$.

However, this approach is not sufficient to define which parts of the free energy function Ψ^{sk} can be recovered. As a matter of fact, this function also depends on other variables, whose possibility of being divided into an elastic and a plastic part must be discussed. In the literature, several options have been explored. Armero [28] and Coussy [19] additively split the Lagrangian fluid mass content m^f into an elastic and plastic part. A variation of this approach is presented by Anand [31], who introduces an additive decomposition of a normalised measure of the variation of the fluid mass, and in Gajo's work [32], where the variation of the fluid content between the current and the initial configuration is additively decomposed. Karrech [4] and Nedjar [14] additively split the Lagrangian porosity ϕ into an elastic and a plastic part. In another work, Nedjar [15] considers the Eulerian porosity n additively decoupled. Physically, the plastic change expressed by these quantities appearing in the literature (mostly related to the porosity) accounts for the irreversible volume variation offered by the particles sliding). In the case of a compressible solid matrix, this mechanism and the irreversible change in volume of the particles are responsible for the total irreversible volume variation, this total value being quantified by J^p.

Despite the different nuances in the approaches proposed by the literature, none of them consider the physical limits of the Eulerian porosity in the range $[0, 1]$, except for Nedjar [14, 15]. Therefore, following Nedjar's model [14], this section considers the additive

decomposition of Lagrangian porosity into an elastic and a plastic part, i.e.,

$$\phi = \phi^e + \phi^p. \tag{11}$$

Hence, in compliance with the hypotheses introduced so far (i.e., a compressible solid skeleton, the multiplicative decomposition of the deformation gradient, the additive decomposition of the Lagrangian porosity, and the physical limits of the Eulerian porosity) the free energy function becomes

$$\Psi^{sk} = \hat{\Psi}^{sk}\left(\boldsymbol{C}^e(\boldsymbol{F}^e), \phi^e, \boldsymbol{\alpha}\right). \tag{12}$$

In the case of an isotropic stress-strain relationship, as in this study work, the dependence of the deformation gradient can be expressed via the left Cauchy-Green strain tensor, i.e.,

$$\Psi^{sk} = \hat{\Psi}^{sk}\left(\boldsymbol{b}^e(\boldsymbol{F}^e), \phi^e, \boldsymbol{\alpha}\right). \tag{13}$$

Owing to the definition (13) of the free energy function, inequality (8) can be rewritten as

$$J\,\mathcal{D}^{sk} = \left(\boldsymbol{\tau} - 2\frac{\partial\hat{\Psi}^{sk}}{\partial\boldsymbol{b}^e}\boldsymbol{b}^e\right) : \boldsymbol{d}^e + \left(p^f - \frac{\partial\hat{\Psi}^{sk}}{\partial\phi^e}\right)\dot{\phi}^e + \boldsymbol{\tau} : \boldsymbol{d}^p + p^f\,\dot{\phi}^p - \frac{\partial\hat{\Psi}^{sk}}{\partial\boldsymbol{\alpha}} * \dot{\boldsymbol{\alpha}} \geq 0, \tag{14}$$

where $*$ indicates the appropriate product operator between the set of conjugate thermodynamical variables $\frac{\partial\hat{\Psi}^{sk}}{\partial\boldsymbol{\alpha}}$ and $\dot{\boldsymbol{\alpha}}$. Inequality (14) makes also use of the standard kinematic relationship $\dot{\boldsymbol{b}}^e = \boldsymbol{l}^e\boldsymbol{b}^e + \boldsymbol{b}^e\,(\boldsymbol{l}^e)^T$, with $\boldsymbol{l}^e \coloneqq \dot{\boldsymbol{F}}^e\,(\boldsymbol{F}^e)^{-1}$.

Following the standard arguments of the Coleman-Noll procedure (see Coleman and Noll [33], and Coleman and Gurtin [34]), the above inequality must hold for any elastic

strain and any elastic porosities, i.e., $\forall \boldsymbol{d}^e \wedge \forall \dot{\phi}^e$, resulting in

$$\begin{cases} \boldsymbol{\tau} = 2\dfrac{\partial \hat{\Psi}^{sk}}{\partial \boldsymbol{b}^e}\boldsymbol{b}^e; & \text{(15a)} \\ p^f = \dfrac{\partial \hat{\Psi}^{sk}}{\partial \phi^e}; & \text{(15b)} \\ J\,\mathcal{D}^{sk} = \boldsymbol{\tau} : \boldsymbol{d}^p + p^f\,\dot{\phi}^p - \dfrac{\partial \hat{\Psi}^{sk}}{\partial \boldsymbol{\alpha}} * \dot{\boldsymbol{\alpha}} \geq 0. & \text{(15c)} \end{cases}$$

Even though correct, the above system does not give any insight on the decomposition of the total stress tensor into two parts, one of which is the so-called *effective* stress. To show how the total stress tensor can be decomposed and by following again Nedjar's [14] work, the skeleton free energy function can be written via the *Legendre transformation* in terms of its dual free energy potential

$$\hat{\Psi}^{sk}\left(\boldsymbol{b}^e, \boldsymbol{\alpha}, \phi^e\right) = X^{sk}\left(\boldsymbol{b}^e, \boldsymbol{\alpha}, p^f\right) + p^f\,\phi^e = X^{'\,sk}\left(\boldsymbol{b}^e, \boldsymbol{\alpha}\right) + X^{por}\left(J^e, p^f\right) + p^f\,\phi^e, \quad (16)$$

where the equation on the right-hand side considers a division of the dual free energy function into a fully drained part (or effective) $X^{'\,sk}$ and a part relative to the pore space, i.e., X^{por}, responsible for maintaining the Eulerian porosity in its physical range. Owing to Eq. (16), Eq. (14) can be re-written as

$$J\,\mathcal{D}^{sk} = \left(\boldsymbol{\tau} - 2\frac{\partial X^{'\,sk}}{\partial \boldsymbol{b}^e}\boldsymbol{b}^e - J^e\frac{\partial X^{por}}{\partial J^e}\boldsymbol{I}^{(2)}\right) : \boldsymbol{d}^e - \left(\phi^e - \frac{\partial X^{por}}{\partial p^f}\right)\dot{p}^f + \boldsymbol{\tau} : \boldsymbol{d}^p + p^f\,\dot{\phi}^p - \frac{\partial X^{'\,sk}}{\partial \boldsymbol{\alpha}} * \dot{\boldsymbol{\alpha}} \geq 0. \quad (17)$$

Applying again the Coleman-Noll procedure, the above inequality must hold for any elastic

strain and any elastic porosities, i.e., $\forall \boldsymbol{d}^e \wedge \forall \dot{\phi}^e$, resulting in

$$\begin{cases} \boldsymbol{\tau} = 2\dfrac{\partial X'^{sk}}{\partial \boldsymbol{b}^e}\boldsymbol{b}^e + J^e \dfrac{\partial X^{por}}{\partial J^e}\boldsymbol{I}^{(2)}; & \text{(18a)} \\ \phi^e = -\dfrac{\partial \hat{\Psi}^{sk}}{\partial p^f}; & \text{(18b)} \\ J\,\mathcal{D}^{sk} = \boldsymbol{\tau} : \boldsymbol{d}^p + p^f\,\dot{\phi}^p - \dfrac{\partial X'^{sk}}{\partial \boldsymbol{\alpha}} * \dot{\boldsymbol{\alpha}} \geq 0. & \text{(18c)} \end{cases}$$

From the above system, it can be seen how the total stress can be additively decomposed into an effective and a porous part, i.e., $\boldsymbol{\tau} = \boldsymbol{\tau}' + \boldsymbol{\tau}^{por}$. In particular, the latter term $\boldsymbol{\tau}^{por}$ is more sophisticated than a term proportional to the fluid pressure (see Nedjar [14] for details). Hence, even though the work proposed by Nedjar [14, 15] is by all means consistent both in terms of thermodynamics and bounded values of Eulerian porosity, it can be understood how a particularly elaborate expression of $\boldsymbol{\tau}^{por}$ increases implementation difficulties. This increase in the level of complexity is notably evident when that expression of $\boldsymbol{\tau}^{por}$ is compared to the well-established and straightforward decomposition of the total stress tensor proposed by Biot [7] for a compressible solid skeleton, i.e., $\boldsymbol{\tau} = \boldsymbol{\tau}' - b\,p^f\boldsymbol{I}^{(2)}$ (with b being the *Biot coefficient*).

Furthermore, Eq. (18c) implies that a law governing the plastic evolution of the porosity is required, i.e., the classical flow rule governing the plastic strains and the internal set of variables are not sufficient. Nedjar [15] defines this evolution law as *yield concept*, respectful of Karush-Kuhn-Tucker (KKT) conditions analogous to the classical yield function ones. Since yield functions governing the strain plasticity have been studied for a long time and the publications to describe different materials are practically countless, it can be understood how yield concepts would require as much work to reach the same level of sophistication as yield functions. Moreover, the definition of the yield concept and its multiplier leads to another non-linear function, whose solution comes with additional computational costs.

2.2. Thermodynamics for incompressible solid matrix

Introducing the hypothesis of incompressibility of the solid matrix has been justified in multiple ways in the literature. The idea has both physical reasons, i.e., the volumetric deformations in the solid matrix are of secondary importance (this is especially true in the case of non-occluded porosity, see Coussy [19], which is one of the hypotheses introduced at the beginning of this section), and mathematical ramifications, as it simplifies the calculations (see, for instance, Bennethum [16]).

Keeping the solid volume constant introduces some kinematic relationships, which are widely recognised in the literature (see [35–38]). Mathematically, these relationships can be expressed in several mutually equivalent ways, i.e., if the infinitesimal solid volumes are considered

$$d\Omega_0^{sk} = d\Omega^{sk}, \tag{19}$$

or, expressing the solid volume fraction via the Eulerian porosity, the above equation becomes

$$(1 - n_0)\, d\Omega_0 = (1 - n)\, d\Omega, \tag{20}$$

where $d\Omega$ and $d\Omega_0$ indicates the infinitesimal current and initial volumes of the mixture. Furthermore, since this current volume of the porous material $d\Omega$ is related to its original counterpart by the Jacobian, the above equation becomes

$$1 - \underbrace{n_0}_{:=\phi_0} = J - \underbrace{J\, n}_{:=\phi}. \tag{21}$$

Using of the equation relating the volumetric part of the logarithmic strain and the Jacobian, the above equation can also be rearranged as follows

$$1 + \phi - \phi_0 = J = \exp \epsilon_v. \tag{22}$$

If the Eulerian porosity is expressed in terms of the Jacobian, then it also follows that

$$n = 1 - \frac{1}{J}\left(1 - n_0\right). \tag{23}$$

In the literature (see, for instance, Coussy [19] or Gajo [32]), the above equation is often computed via solid mass conservation, having imposed constant density. Thus, at constant density (assumed by solid matrix incompressibility), disregarding Eq. (23) implies the violation of the solid mass conservation.

From Eq. (22) and (23), it can be appreciated how considering the solid matrix as incompressible creates a relationship between the measures of the porosity and the Jacobian (or volumetric part of the logarithmic strain). Being the Eulerian porosity physically bounded in the range $(0, 1)$, these constraints affect the admissible values of the Jacobian. These considerations have several consequences, the first one being that the porosity and the deformation gradient are not two independent variables as in the case of a compressible solid matrix. Therefore, Eq. (9) becomes

$$\Psi^{sk} = \hat{\Psi}^{sk}_{inc}\left(\boldsymbol{F}, \boldsymbol{\alpha}\right) = \hat{\Psi}^{sk}_{inc}\left(\boldsymbol{C}, \boldsymbol{\alpha}\right), \tag{24}$$

where the equation on the right-hand side is introduced for a matter of objectivity, as previously for Eq. (10).

Another consequence of the above-introduced hypothesis regards the decomposition of the quantity of interest into an elastic and a plastic part. In particular, if the multiplicative decomposition of the deformation gradient is considered again, the decomposition of the Jacobian is given by $J = J^e\, J^p$. From the rate of Eq. (22), it can be seen that

$$\begin{aligned} \dot{J} = \dot{\phi} = J\,\dot{\epsilon}_v = \;& J\,\boldsymbol{I}^{(2)} : \boldsymbol{d}; \\ \left(J^e\, J^p\right)^{\cdot} = \left(\phi\right)^{\cdot} = J^e\, J^p \;& \left(\dot{\epsilon}^e_v + \dot{\epsilon}^p_v\right) = J^e\, J^p \boldsymbol{I}^{(2)} : \left(\boldsymbol{d}^e + \boldsymbol{d}^p\right), \end{aligned} \tag{25}$$

with $(\bullet)^{\cdot}$ being the rate of the whole quantity $(\bullet)$ between the brackets. From Eq. (25), it can be understood that the Lagrangian porosity rate must match the Jacobian rate, implying that a change in the whole volume must correspond to a change in the volume of the fluid constituent, as expected. However, Eqs. (22) and (25) show that there is no one-to-one correspondence between the elastic or plastic Jacobian and the elastic or plastic Lagrangian porosities, either in terms of finite or rate forms, i.e.,

$$\phi^e \neq J^e, \qquad \phi^p \neq J^p; \tag{26}$$

$$\dot{\phi}^e \neq \dot{J}^e, \qquad \dot{\phi}^p \neq \dot{J}^p. \tag{27}$$

The above equations comply with the physical explanation: if the compressibility of the solid phase is not considered, only the particles sliding contribute to the total volume variation, tracked by J, and decomposed into an elastic and plastic part. Therefore, in this model accounting for the incompressibility of the solid phase, the Lagrangian porosity is a proxy only of the free volume filled by the water.

As discussed in Section 2.1, let the considered solid skeleton be isotropic. To consider the kinematic relationship (22) (or, equally, (23)) between the Jacobian and the porosity, and, simultaneously, accounting for the impossibility of decomposing the latter (i.e., the porosity) into an elastic and plastic part, the free energy function must be expressed as

$$\Psi^{sk} = \hat{\Psi}^{sk}_{inc}\left(\boldsymbol{b}^e, \boldsymbol{b}^p, \boldsymbol{\alpha}\right). \tag{28}$$

The above equation underlies how the dependency from the whole strain tensor is required to account for a material being dependent from the porosity.

For the case of incompressible solid matrix, the solid skeleton part of the Clausius-

Duhem inequality (8) becomes

$$J\,\mathcal{D}^{sk} = \left(\boldsymbol{\tau} + Jp^f\,\boldsymbol{I}^{(2)} - 2\frac{\partial\hat{\Psi}^{sk}_{inc}}{\partial\boldsymbol{b}^e}\boldsymbol{b}^e\right) : \boldsymbol{d}^e + \left(\boldsymbol{\tau} + Jp^f\,\boldsymbol{I}^{(2)}\right) : \boldsymbol{d}^p - 2\frac{\partial\hat{\Psi}^{sk}_{inc}}{\partial\boldsymbol{b}^p}\dot{\boldsymbol{b}}^p - \frac{\partial\hat{\Psi}^{sk}_{inc}}{\partial\boldsymbol{\alpha}} * \dot{\boldsymbol{\alpha}} \geq 0, \tag{29}$$

where Eq. (25) is used to express the rate of the Lagrangian porosity as rate of the Jacobian.

Before applying the Coleman-Noll procedure, which does not account for any restriction in the adopted strain measure, the above-mentioned consequences of the kinematic relationship (23) must be considered. Since the Eulerian porosity is physically bounded by the inequalities $0 < n < 1$, these can also be expressed in terms of the volumetric logarithmic strain[4] via Eq. (22), i.e.,

$$\begin{cases} \epsilon_v > \ln\left(1 - n_0\right); & \text{(30a)} \\ \dfrac{1}{\exp\left(\epsilon_v\right)}\left(1 - n_0\right) > 0. & \text{(30b)} \end{cases}$$

While the latter of the above inequalities is always satisfied (the initial Eulerian porosity satisfies $0 < n_0 < 1$), the former is not. Inequality (30a) imposes a constraint on the negative (i.e., compression) values of the volumetric logarithmic strain. If expressed in terms of the Jacobian, (30a) gives $J > (1 - n_0)$, which is more restrictive that the usually considered $J > 0$ for the standard mechanics of solids. Violation of (30a) leads to negative values of the Eulerian porosity and, as motivated above, to violating the solid mass conservation.

Given the restriction in (30a), the Coleman-Noll procedure can be applied to (29),

[4]Inequalities (30) are expressed in terms of logarithmic strain since Section 3 will discuss their implications for a *Hencky* material, i.e., a material describing a stress-strain relationship between the Kirchhoff stress and the logarithmic strain. Nothing prevents expressing the inequalities inherited from the physical constraints on the Eulerian porosity as a function of other strain measures.

resulting in

$$\begin{cases} \boldsymbol{\tau}' = 2\dfrac{\partial \hat{\Psi}^{sk}_{inc}}{\partial \boldsymbol{b}^e}\boldsymbol{b}^e; & \text{(31a)} \\ J\,\mathcal{D}^{sk} = \boldsymbol{\tau}' : \boldsymbol{d}^p - 2\dfrac{\partial \hat{\Psi}^{sk}_{inc}}{\partial \boldsymbol{b}^p}\dot{\boldsymbol{b}}^p - \dfrac{\partial \hat{\Psi}^{sk}_{inc}}{\partial \boldsymbol{\alpha}} * \dot{\boldsymbol{\alpha}} \geq 0; & \text{(31b)} \\ \epsilon_v > \ln\left(1 - n_0\right), & \text{(31c)} \end{cases}$$

where the introduction of the *Terzaghi effective* stress defined as

$$\boldsymbol{\tau}' \coloneqq \boldsymbol{\tau} + Jp^f \boldsymbol{I}^{(2)}, \tag{32}$$

naturally derives from the Clausius-Duhem inequality (29) and the hypothesis of solid matrix incompressibility. The decomposition of the total stress tensor into an effective and a fluid pressure part has been widely used in the literature (see, for instance, [39] for the introduction of this idea in the small strain theory and [40] for its adaptation to the finite strain case), both for its simplicity and its compliance with the laws of thermodynamics. Eqs. (31a) and (31b) fit into the framework of hyper-plastic formulations (see the work of Collins and co-workers [41–49]), provided that a dissipation function $J\,\mathcal{D}^{sk} \geq 0$ is introduced. The compliance of this inequality with the principles of hyper-plasticity is briefly summarised in Appendix B.1.

3. A new incompressibility-compliant free energy function

While (31a) and (31b) constitute the classical equations for (hyper-)elasto-plasticity, an implementation that has incompressibility of the solid matrix as its founding assumption must include (31c) too. In the literature, multiple ways exist to include constraints, such as the penalty method or the Lagrange multiplier, to name the most popular ones. However, these methods add terms to the primary equations (and primary unknowns too in the case of the Lagrange multiplier), making them less attractive, especially if these primary equations require a linearisation to be solved implicitly. As suggested in Section 2.1, another

potential way forward to include (31c) is via a modification of the free energy function. Such an amendment can be easily applied to materials exhibiting a free energy function energy given by the sum of a volumetric and a deviatoric part (these materials have firstly been proposed by Flory [50]). In particular, the inclusion of constraint (31c) can be ensured if the volumetric part of the free energy function contains these two features:

- it has a vertical asymptote for values of the volumetric strain approaching the constraint, i.e., $\lim_{\epsilon_v \to \ln(1-n_0)^+} \hat{\Psi}^{sk}_{inc}(\epsilon_v) = +\infty$;
- it is not defined for the volumetric deformations excluded by constraint (31c), being these inadmissible by the incompressibility assumption, i.e., $\hat{\Psi}^{sk}_{inc}(\epsilon_v) : \epsilon_v \in (\ln(1-n_0), +\infty) \to \mathbb{R}$.

This work considers a free energy function of a *Hencky* material and accommodates it to comply with the above-listed requirements, resulting in the following formula

$$\hat{\Psi}^{sk}_{inc}(\boldsymbol{\epsilon}, \boldsymbol{\alpha}) = \frac{K}{2\,n}\left(\epsilon^e_v\right)^2 + \frac{3}{2}G\left(\epsilon^e_q\right)^2 + \tilde{\Psi}^{sk}_{inc}(\boldsymbol{\alpha}(n)), \tag{33}$$

with $K > 0$ and $G > 0$. In the above equation, K is the (constant) bulk parameter (in contrast to the (tangent) bulk modulus, which will be discussed in the following section), G is the shear modulus and $\epsilon_q \coloneqq \sqrt{\frac{2}{3}\,\boldsymbol{e} : \boldsymbol{e}}$ is the *von-Mises* equivalent strain, with $\boldsymbol{e} \coloneqq \boldsymbol{\epsilon} - \frac{\epsilon_v}{3}\boldsymbol{I}^{(2)}$ being the deviatoric part of the strain tensor. Due to the modification introduced, the material described by Eq. (33) will henceforth be called *improved* Hencky material. It must be recognised that a similar adaption (i.e., scaling the bulk modulus with the inverse of the Eulerian porosity) modulus can be applied to other kinds of materials, such as the compressible versions of neo-Hookean or Mooney-Rivlin material (see, for instance, de Souza Neto *et al.* [25]). However, these modifications are beyond the scope of this work, which focuses on the improved Hencky material.

A few considerations on the free energy function introduced by Eq. (33) can be made:

- A similar constitutive model considering the dependence of the effective stress on the porosity has been proposed by Nordstrom *et al.* [51] and Hewitt *et al.* [52] in the context of the small strain setting for the mono-dimensional case. The above formulation represents an extension to the three-dimensional finite strain case accounting for (hyper) elasto-plasticity. The above models are also supported by laboratory tests, thus enabling the proposed formulation to be thoroughly supported by laboratory tests and theoretical self-consistency;

- the deviatoric part of the energy is unmodified compared to the linear *Hencky* material. Keeping the shear modulus constant is not a unique choice, since the literature has proposed materials with a constant Poisson's ratio and a variable bulk modulus. Nonetheless, as pointed out by Zytinsky *et al.* [53] a material with these features is non-conservative, thus non hyper-elastic. Moreover, such a material would fail to reproduce an asymptotically incompressible material, as the Poisson's ratio should asymptotically tend to 0.5 in this case (see, in this regards, Figure 2d);

- as Eq. (33) is a modification of a Hencky material, it suffers from drawbacks similar to its original formulation. In particular, it is well-known that the free energy function of a Hencky material is not poly-convex but only convex, as it can be appreciated from Figures 2a and 3a), and as pointed out, for instance, by Simo [30, 54]. This leads to issues in the case of large elastic strains (see, for instance, [55] or [56] for discussions on this matter). However, as typical for geo-materials, a prominent role is played by plastic strains, relegating elastic range to a secondary status;

- it can be noticed that Eq. (33) cannot be written in the form of a *decoupled* or *uncoupled* material, defined as $\Psi^{sk} = \Psi_1^{sk}(\boldsymbol{b}^e) + \Psi_2^{sk}(\boldsymbol{b}^p)$. These materials were first described by Lubliner [57]. In particular, Eq. (33) defines a material exhibiting *modulus coupling*, which, to be in compliance with the laws of thermodynamics, requires a non-associated flow rule (this is detailed in Appendix B.1, but, for a com-

plete treatment of this subject, the reader is referred to Collins and Houlsby [41] and Collins [58]). In the case of elasto-plastic behaviour, this coupling causes a dependency of the effective stress response on the plastic strain, which, as previously mentioned in Section 2.2, stems from the impossibility of decomposing the porosity into an elastic and plastic part. This coupling result, stemming from theoretical considerations, is further supported by laboratory tests with hydrogel particles (see Hewitt *et al.* [52]). These experiments found that a hysteresis loop is created for increasing and decreasing fluid pressure. For these different fluid pressure values, the steady state is fully achieved, and strain values vary accordingly, thus fostering the notion that effective stress must consider a dependency on plastic phenomena to reproduce the hysteretic behaviour;

- this specific feature describing the dependency of the elastic moduli on a bounded parameter (i.e., the Eulerian porosity in the case of Eq. (33)) bears some similarities with damage mechanics (see Houlsby and Puzrin [59] for a thermodynamical background and Murakami [60] for a detailed explanation). In the context of damage mechanics, the damage parameter (or damage variable), which varies between 0 and 1, makes the stress response vary between the undamaged state of the considered sample and the entirely damage status;

- conceptually speaking, the model described by Eq. (33) provides a stiffening of the volumetric behaviour in the case of compression, i.e., when the ejection of water from the sample makes the material progressively similar only to its solid constituent, this being, by assumption, is incompressible. This idea of increasing volumetric stiffness is in compliance with other non-linear models available in the literature for the finite strain theory in geo-mechanics (see, for instance, the models in [61]). However, when the incompressibility of the solid phase is introduced, a stiffening behaviour of the bulk modulus during a volumetric compression phase is not sufficient to respect constraint (31c).

3.1. Stress computation for elastic strain

In this section, the stress state is computed only taking elastic deformations into account, i.e., $\boldsymbol{F} = \boldsymbol{F}^e$. Calculations are detailed in Appendix A.1.

If the free energy function introduced by Eq. (33) is considered, Eq. (31a) becomes

$$\boldsymbol{\tau}' = \frac{\partial \hat{\Psi}^{sk}_{inc}}{\partial \boldsymbol{\epsilon}^e} = \underbrace{\frac{K\,\epsilon_v^e}{n}\left(1 + \frac{\epsilon_v^e}{2\,n}\,(n-1)\right)}_{:=p'}\boldsymbol{I}^{(2)} + \underbrace{2G\,\bar{\boldsymbol{e}}^e}_{:=\boldsymbol{s}}, \tag{34}$$

where Eqs. (A.1)- (A.4) are used. In compliance with Eq. (32), effective deviatoric parts match their total counterparts. As such, the superscript $(\bullet)'$ is dropped for these quantities.

The plots of the volumetric part of the free energy function as well as its first derivative with respect to ϵ_v^e (i.e., the pressure part of effective Kirchhoff stress p') are illustrated in Figures 2a and 2b. Both these figures and Eq. (34) clearly show that, in terms of p', the improved Hencky material becomes progressively similar to the original Hencky as $n \to 1^-$. This serves exactly the purpose of this work, namely modifying the free energy function in correspondence of inadmissible strain values, while maintaining the behaviour of the original material far from this limit.

As the model is non-linear in terms of strain, it is necessary to compute the incremental stress-strain relationship to study the tangent moduli. Hence, if the rate of Eq. (34) is considered, it follows that

$$d\boldsymbol{\tau}' = \underbrace{\frac{\partial^2 \hat{\Psi}^{sk}_{inc}}{\partial \boldsymbol{\epsilon}^e \otimes \partial \boldsymbol{\epsilon}^e}}_{:=\boldsymbol{\mathcal{D}}^e} : d\boldsymbol{\epsilon}^e = \left(K^{e,\,tan}\,\boldsymbol{I}^{(2)} \otimes \boldsymbol{I}^{(2)} + 2\,G\,\boldsymbol{I}^{(4),\,dev}\right) : d\boldsymbol{\epsilon}^e, \tag{35}$$

with

$$K^{e,\,tan} := \frac{K}{2\,n^3}\left(n^2\left((\epsilon_v^e)^2 + 4\,\epsilon_v^e + 2\right) - \epsilon_v^e\,n\,(3\,\epsilon_v^e + 4) + 2\,(\epsilon_v^e)^2\right). \tag{36}$$

Full expression of $\boldsymbol{I}^{(4),\,dev}$ appearing in Eq. (35) is given by Eq. (A.7). Limits for the

extremes values of the Eulerian porosity give (see also Figure 2c)

$$\lim_{n\to 0^+} K^{e,\,tan} = +\infty; \tag{37}$$

$$\lim_{n\to 1^-} K^{e,\,tan} = K, \tag{38}$$

which reaffirm the idea discussed above about the proposed modification.

Known the tangent elastic bulk modulus and the constant shear modulus, the tangent elastic Poisson's ratio can be computed as usual for isotropic materials, i.e.,

$$\nu^{e,\,tan} := \frac{3K^{e,\,tan} - 2G}{2\left(3K^{e,\,tan} + G\right)}, \tag{39}$$

where, for the extremes values of the Eulerian porosity, it can be seen that (see also Figure 2d)

$$\lim_{n\to 0^+} \nu^{e,\,tan} = \frac{1}{2}; \tag{40}$$

$$\lim_{n\to 1^-} \nu^{e,\,tan} = \frac{3K - 2G}{2\left(3K + G\right)}. \tag{41}$$

3.2. Stress computation for elasto-plastic strain

This section recovers the full hypothesis introduced in Section 2, where elastic and plastic strains are considered, i.e., $\boldsymbol{F} = \boldsymbol{F}^e\,\boldsymbol{F}^p$. Some further details on the implementation of an elasto-plastic subroutine are given in Appendix A.2.

As previously mentioned in Section 2.2, the introduction of a dissipation function $J\,\mathcal{D}^{sk}$, by means of which a yield function $\Phi^{\tau'}$ and a flow rule g can be described, makes the formulation consistent with the basic principles of hyperplasticity. Therefore, in this work, it is assumed that $\Phi^{\tau'}$ and g are given once $J\,\mathcal{D}^{sk}$ is introduced. An example of this calculatiation is provided in Appendix B.2. Furthermore, as including a further hardening rule would not provide any further insight on the implementation of the current free energy func-

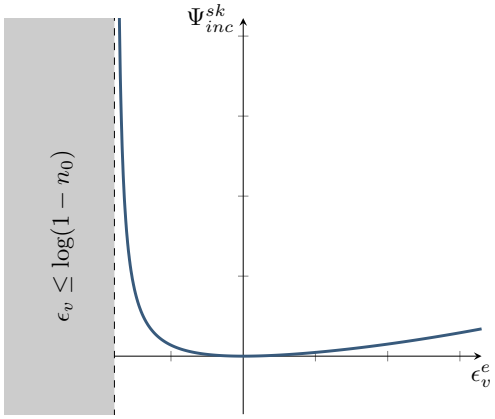

(a) Volumetric part of the free energy function.

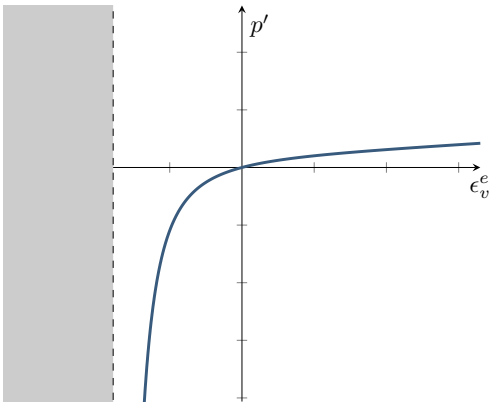

(b) Effective Kirchhoff pressure.

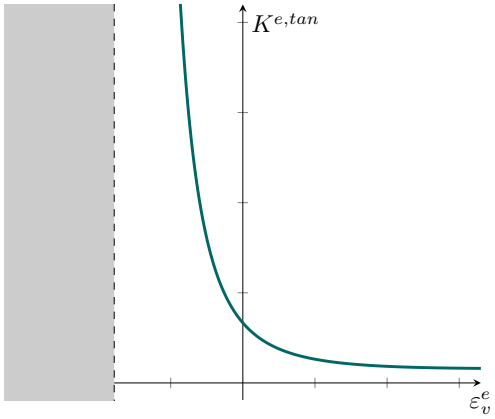

(c) Tangent elastic bulk modulus.

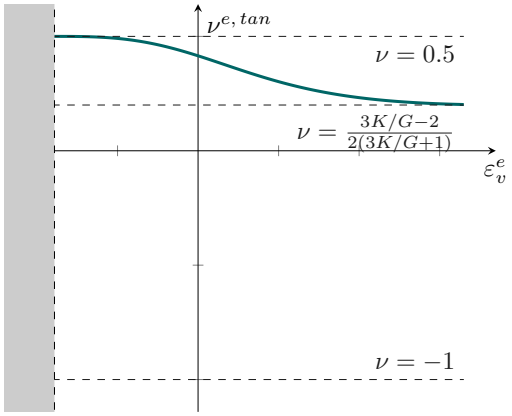

(d) Tangent Elastic Poisson' ratio.

Figure 2: Bi-dimensional plots for the elastic case. Grey-shaded areas indicate where (31c) is not respected.

tion, this is not considered here, i.e., $\tilde{\Psi}^{sk}_{inc}(\boldsymbol{\alpha}) = 0$. Given these hypotheses, the standard equations for implementing a stress-strain subroutine are given by the (time-discretised) decomposition in the logarithmic strain space resembling the small-strain additive decomposition, and by the satisfaction of the yield function for the stress tensor, i.e.,

$$\begin{cases} \boldsymbol{\epsilon}^e - \boldsymbol{\epsilon}^{e,tr} + \Delta\gamma \dfrac{\partial g}{\partial \boldsymbol{\tau}'} = \mathbf{0}; & \text{(42a)} \\ \Phi^{\tau'}\left(\boldsymbol{\tau}'\right) = 0, & \text{(42b)} \end{cases}$$

where $\Delta\gamma \geq 0$ is the increment in the plastic multiplier, which, along with $\Phi^{\tau'}(\boldsymbol{\tau'}) \leq 0$ and the compatibility condition $\Phi^{\tau'}\,\Delta\gamma = 0$, gives the classical KKT conditions. Since the above system of equations cannot be solved analytically, its linearisation with respect to the unknown quantities (with the elastic trial strain an unknown in this case) is performed, this being

$$\begin{cases} d\boldsymbol{\epsilon}^e - d\boldsymbol{\epsilon}^{e,\,tr} + d\Delta\gamma\,\dfrac{\partial g}{\partial \boldsymbol{\tau'}} + \Delta\gamma\,\dfrac{\partial^2 g}{\partial \boldsymbol{\tau'} \otimes \partial \boldsymbol{\tau'}} : d\boldsymbol{\tau'} = \boldsymbol{0}; & \text{(43a)} \\ \dfrac{\partial \Phi^{\tau'}}{\partial \boldsymbol{\tau'}} : d\boldsymbol{\tau'} = 0. & \text{(43b)} \end{cases}$$

As can be seen from the above equations, the computation of the stress increment $d\boldsymbol{\tau'}$ becomes necessary. According to Eq. (33) and considering the elastic and plastic strains describing the whole sets of unknowns, the stress increment can be written as follows

$$d\boldsymbol{\tau'} = \underbrace{\frac{\partial^2 \hat{\Psi}^{sk}_{inc}}{\partial \boldsymbol{\epsilon}^e \otimes \partial \boldsymbol{\epsilon}^e}}_{=\boldsymbol{\mathcal{D}}^e} : d\boldsymbol{\epsilon}^e + \underbrace{\frac{\partial^2 \hat{\Psi}^{sk}_{inc}}{\partial \epsilon^p_v\, \partial \boldsymbol{\epsilon}^e} \otimes \boldsymbol{I}^{(2)}}_{=\boldsymbol{\mathcal{D}}^p} : \left(\underbrace{d\Delta\gamma\,\frac{\partial g}{\partial \boldsymbol{\tau'}} + \Delta\gamma\,\frac{\partial^2 g}{\partial \boldsymbol{\tau'} \otimes \partial \boldsymbol{\tau'}} : d\boldsymbol{\tau'}}_{=d\boldsymbol{\epsilon}^{e,\,tr} - d\boldsymbol{\epsilon}^e} \right), \tag{44}$$

where

$$\boldsymbol{\mathcal{D}}^p := \frac{\partial^2 \hat{\Psi}^{sk}_{inc}}{\partial \epsilon^p_v\, \partial \boldsymbol{\epsilon}^e} \otimes \boldsymbol{I}^{(2)} = \underbrace{\frac{K}{2}\left(\frac{\epsilon^e_v}{n}\right)^2 (1-n)\left(1 + \frac{2}{n}(1-n)\right)}_{:=K^{p,\,tan}} \boldsymbol{I}^{(2)} \otimes \boldsymbol{I}^{(2)}. \tag{45}$$

The second term in Eq. (44) shows the above-mentioned coupling between the elastic and plastic parts of the free energy function taking place via the Eulerian porosity. As Eq. (45) and Figure 3 highlight, this coupling phenomenon is purely volumetric.

From Eq. (44), the effective stress can be isolated, i.e.,

$$\left(\boldsymbol{I}^{4,\,sym} - \Delta\gamma\,\boldsymbol{\mathcal{D}}^p : \frac{\partial^2 g}{\partial \boldsymbol{\tau'} \otimes \partial \boldsymbol{\tau'}} \right) : d\boldsymbol{\tau'} = \boldsymbol{\mathcal{D}}^e : d\boldsymbol{\epsilon}^e + d\Delta\gamma\,\boldsymbol{\mathcal{D}}^p : \frac{\partial g}{\partial \boldsymbol{\tau'}}, \tag{46}$$

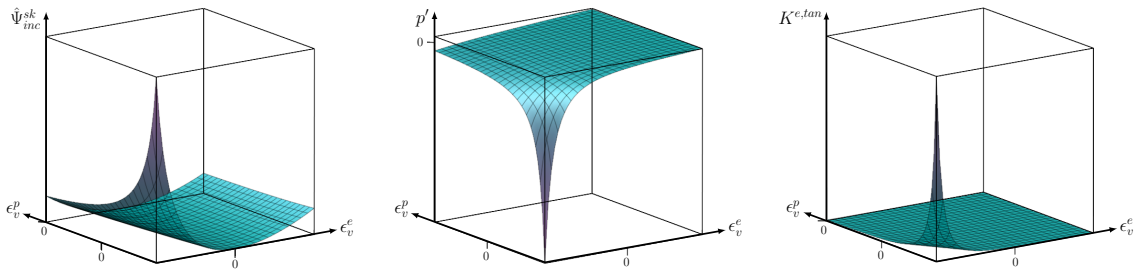

(a) Volumetric part of the free energy function.

(b) Effective Kirchhoff pressure.

(c) Tangent elastic bulk modulus.

Figure 3: Three-dimensional plots of the volumetric parts described by Eq. (33), and its first and second derivatives with respect to ϵ^e_v.

where it is convenient to define the above-appearing fourth-order tensor as

$$\mathbf{\Upsilon} \coloneqq \left(\boldsymbol{I}^{4,\,sym} - \Delta\gamma\, \boldsymbol{\mathcal{D}}^p : \frac{\partial^2 g}{\partial \boldsymbol{\tau}' \otimes \partial \boldsymbol{\tau}'} \right)^{-1}. \tag{47}$$

Hence, Eq. (46) becomes

$$d\boldsymbol{\tau}' = \mathbf{\Upsilon} : \boldsymbol{\mathcal{D}}^e : d\boldsymbol{\epsilon}^e + d\Delta\gamma\, \mathbf{\Upsilon} : \boldsymbol{\mathcal{D}}^p : \frac{\partial g}{\partial \boldsymbol{\tau}'}. \tag{48}$$

The above equation can be directly substituted into Eqs. (42), giving

$$\begin{cases} d\boldsymbol{\epsilon}^e - d\boldsymbol{\epsilon}^{e,\,tr} + d\Delta\gamma \dfrac{\partial g}{\partial \boldsymbol{\tau}'} + \Delta\gamma \dfrac{\partial^2 g}{\partial \boldsymbol{\tau}' \otimes \partial \boldsymbol{\tau}'} : \left(\mathbf{\Upsilon} : \boldsymbol{\mathcal{D}}^e : d\boldsymbol{\epsilon}^e + d\Delta\gamma\, \mathbf{\Upsilon} : \boldsymbol{\mathcal{D}}^p : \dfrac{\partial g}{\partial \boldsymbol{\tau}'} \right) = \mathbf{0}; & \text{(49a)} \\ \dfrac{\partial \Phi^{\tau'}}{\partial \boldsymbol{\tau}'} : \left(\mathbf{\Upsilon} : \boldsymbol{\mathcal{D}}^e : d\boldsymbol{\epsilon}^e + d\Delta\gamma\, \mathbf{\Upsilon} : \boldsymbol{\mathcal{D}}^p : \dfrac{\partial g}{\partial \boldsymbol{\tau}'} \right) = 0. & \text{(49b)} \end{cases}$$

Iterative solutions to (49) allow computation of the elastic strains and the plastic multiplier. These, in turn, permit the computation of the effective stress via Eq. (48).

The original uncoupled Hencky material can be recovered by setting $\boldsymbol{\mathcal{D}}^p$ as zero in Eq. (47), which also gives $\mathbf{\Upsilon} = \boldsymbol{I}^{4,\,sym}$.

4. Numerical examples

The proposed stress-strain relationship has been implemented into a Material Point Method (MPM) framework (outlined by Charlton *et al.* [62] and based AMPLE [63] code) and extended to porous materials, which is briefly introduced in Section 4.1. Section 4.2 takes a column under self-weight into account, where the new model is benchmarked against a classical linear Hencky material in the elastic case. The analyses described in Section 4.3 consider an elasto-plastic behaviour (both for the current model and the linear Hencky material) for a deformable footing problem in $3D$, emphasising that the new model is not only necessary but also applicable to routinary geotechnical simulations.

4.1. Implementation into an implicit Material Point Method formulation

The stress-strain relationship defined by Eq. (34) for the elastic case, and by the iterative linear system (A.9) for the elasto-plastic case, has been implemented into an implicit Material Point Method (MPM) $\boldsymbol{u}-p^f$ formulation, with one set of material points [5]. The choice of implementing the new constitutive model into an MPM framework, avoids mesh distortions, which can occur with large deformations. However, this choice does not confine the new model to large deformations as inequality (31c) can also be violated for moderate deformations. The used formulation has been cast in a similar way to that proposed by Zhao and Choo [65], with the following differences:

- water has been considered as a barotropic fluid. Hence, the fluid phase has been modelled as a slightly-compressible material according to the law $\dot{\rho^f} = \frac{\rho^f}{K^f}\dot{p^f}$ (in compliance with Eq. (6)), with K^f being the bulk modulus of the fluid part;
- viscosity effects are not considered for the current model, in contrast to Zhao and Choo [65];

[5] The so-called $\boldsymbol{u}-p$ indicates the primary variables used in the coupled formulation, i.e., the solid phase displacement $\boldsymbol{u}$ and the fluid pressure p^f. The reader is referred to [64] for a detailed discussion on porous material formulations and number of Material Point sets in the MPM.

Table 1: Summary of the parameters considered in the analyses of the elastic column under self-weight.

Solid phase		Fluid phase	
G	$3 \cdot 10^5$ Pa	K^f	$2.2 \cdot 10^9$ Pa
ρ^{sk}	2650 kg m^{-3}	ρ_0^f	1000 kg m^{-3}
Porous material			
	κ_0		$1 \cdot 10^{-5}$ m s^{-1}
	n_0		0.3

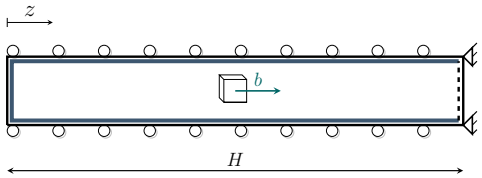

Figure 4: Illustration of the elastic column under self-weight.

- hydraulic conductivity κ varies according to the Kozeny-Carman formula (following the approach proposed by Bandara and Soga [66]), i.e.,

$$k\,\rho^f\,g = \kappa = c_1 \frac{n^3}{(1-n)^2}, \tag{50}$$

  with c_1 being a constant parameter and g the value of gravity;

- the consistent mass matrix has been used in lieu of the lumped one (for a definition of these in the context of the MPM the reader is referred to [67]).

The shape functions used for the simulations are those employed in the Generalised Interpolation Material Point Method (GIMPM), originally proposed by Bardenhagen *et al.* [68]), and here defined as suggested by Zhao and Choo [65] for the $\boldsymbol{u}-p^f$ formulation. The parameters used in the following analyses relative to the fluid part represent water. Those relative to the solid skeleton are not distinctive of a specific material, but they span a range of values that interest geomechanics.

4.2. Elastic column under self-weight

As a first example, the elastic column under gravitational load shown in Figure 4 is considered. Roller boundary conditions are applied to the upper and lower sides of the column, with the right surface being fixed and the left surface free. In addition, the entire external surface is impermeable, except for the right part, where zero atmospheric pressure

is prescribed. The whole simulation is run using a quasi-static formulation for $3,000$ pseudo time-steps, and the gravitational load is increased linearly for the first $1,000$ steps and kept constant for the remaining time. The selected gravitation[6] reaches $b = 1,000$ m s^{-2}. The height H of the column is 1 m, discretised by 20×1 elements, each of which is initially populated by 4^2 material points. The other hydro-mechanical parameters considered in the simulation are listed in Table 1.

As it can also be noticed in Table 1, the bulk parameter is not given. The reason lies in the comparison between an original linear Hencky material with the proposed model characterised by a porosity-dependent volumetric behaviour expressed by Eq. (33). The bulk modulus for the linear Hencky material $\bar{K}$ has been set so that it matches the initial elastic tangent bulk modulus $K_0^{e,tan}$ defined by Eq. (36), i.e., it has been computed in correspondence of initial porosity n_0 and zero elastic volumetric strain, i.e., $K = \bar{K}\, n_0 = 5 \cdot 10^5$ Pa. In this fashion, the stiffness of the two materials is initially the same.

Figure 5 shows time-plots for different quantities comparing the two simulations. In particular, for the analysis where the original Hencky material is considered, time $\tilde{t}$ (corresponding to the 157^{th} pseudo time-step) highlights the watershed between positive and negative values of the Eulerian porosity (see Figure 5a, but also Figure 6a). From a physical perspective, it is clear that the simulation using the original Hencky material cannot be regarded as valid after $\tilde{t}$. Nonetheless, it can be noticed from Figures 5c and 5d how the values of primary variables, i.e., displacement $\boldsymbol{u}$ and fluid pressure p^f, differ consistently even for pseudo time-steps lower than $\tilde{t}$. The two models exhibit different behaviour even far from where more significant values of the deformation gradient. Thus, it can be seen how imposing constrained porosity values affects the entire simulation, leading to

[6]The reason for selecting such a substantial gravitational load lies in the drastic reduction of simulation time, especially in correspondence with low hydraulic conductivity values such as the one considered in this example (see Table 1). As the difference between the modified and the original Hencky model concerns the effective stress, the selected gravity accelerates the draining process of the sample, reducing the computational time.

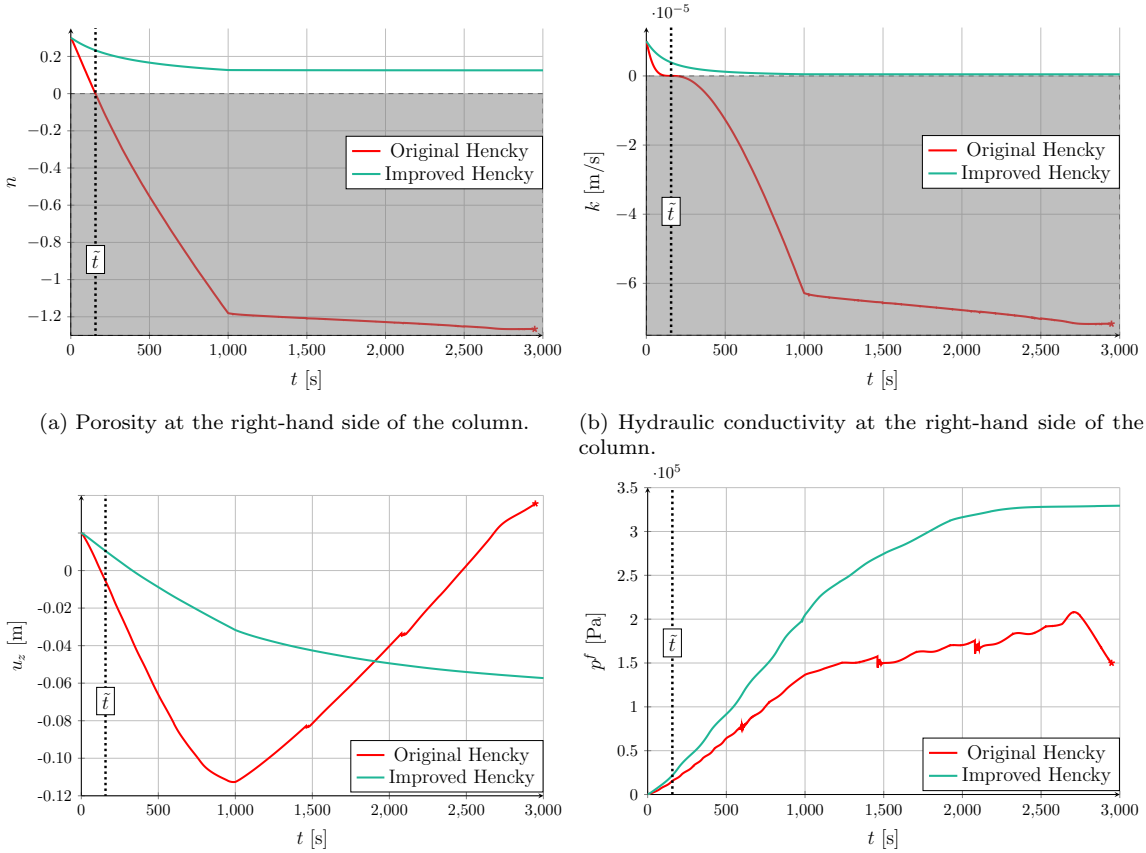

(a) Porosity at the right-hand side of the column.

(b) Hydraulic conductivity at the right-hand side of the column.

(c) Horizontal displacement at the left-hand side of the column.

(d) Fluid pressure at the left-hand side of the column.

Figure 5: Time-plots for different quantities calculated at the right-hand side (top row) and left-hand side (bottom row) of the column under self-weight. Grey-shaded areas indicate the physically unfeasible regions.

very different behaviour even for those parts of the body where such constraints are not expected to be violated (such as the left-hand side of the column). This idea is further illustrated in Figures 5c and 6c: when the simulation continues even for the original Hencky material, it begins to swell to the left (in a direction opposite to gravity). It is rather surprising that the classic Hencky material can continue the simulation in correspondence with extremely low and negative values of hydraulic conductivity without failing. The loss of the positive-definitiveness of the bottom-right matrix of the linearised system comes with the loss of guarantee on the existence and the uniqueness of the solution (see Boffi

et al. [69], Proposition 4.3.1). However, the Newton-Raphson iterative algorithm can still find a solution, and this is likely due to the problem's setup, mainly its simplicity and over-constrained nature (the problem is practically mono-dimensional). However, as can be appreciated from Figures 5c and 5d, the solution fields are notably unstable in several places, and, in the end, a solution cannot be reached at the 2948^{th} pseudo time-step. On the contrary, the new model behaves in accordance with the bounded porosity values and results in smoother transitions on both sides of the column, as highlighted by all of the time-plots of the different quantities in Figure 5. A more uniform deformation state also emerges when comparing the Eulerian porosity values (and thus the Jacobian via Eq. (23)) between Figures 6a-6b at the 157^{th} pseudo time-step, and Figures 6c-6d at the end of the simulations.

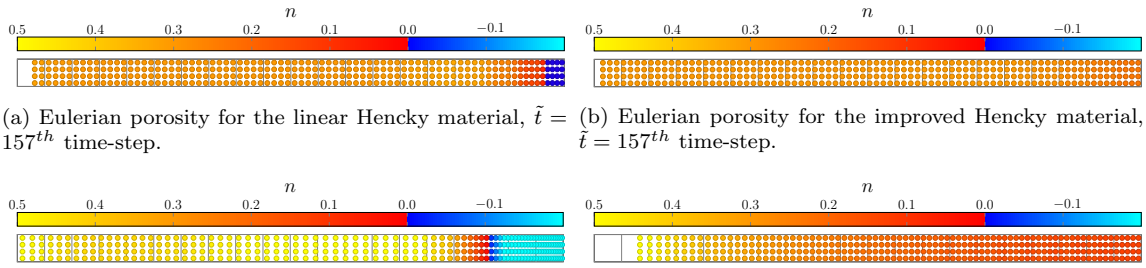

(a) Eulerian porosity for the linear Hencky material, $\tilde{t} = 157^{th}$ time-step.

(b) Eulerian porosity for the improved Hencky material, $\tilde{t} = 157^{th}$ time-step.

(c) Eulerian porosity for the linear Hencky material, final time-step.

(d) Eulerian porosity for the improved Hencky material, final time-step.

Figure 6: Deflection shapes of the columns at $\tilde{t} = 157^{th}$ time-step and the end of each simulation.

4.3. 3D flexible footing

This section considers a $3D$ flexible footing problem in the finite elasto-plastic regime. Computation of the yield function and direction of the plastic flow for the considered model and in compliance with hyper-plasticity are given in Appendix B.2 for the improved Hencky material. The same procedure can be trivially followed for the original Hencky material, which results in associated flow rule.

Since the problem presents two symmetry planes, only a quarter of the whole setup (as represented in Figure 7) is considered. All planes defining the soil boundaries have

Table 2: Summary of the shared parameters considered in the analyses of the elasto-plastic flexible footing under large deformations.

Dimensions			
L_x, L_y, L_z	10 m, 14 m, 10 m		
h_x, h_y, h_z	0.5 m, 0.5 m, 0.5 m		
a	2.5 m		
l_y	10 m		
Solid phase		Fluid phase	
G	$28 \cdot 10^6$ Pa	K^f	$2.2 \cdot 10^9$ Pa
ρ^{sk}	2650 kg m^{-3}	ρ_0^f	1000 kg m^{-3}
Porous material			
κ_0	$1 \cdot 10^{-2}$ m s^{-1}		
Plastic parameters			
p_c	$-250 \cdot 10^5$ Pa		
α, γ	0.3, 0.9		
M	0.964		

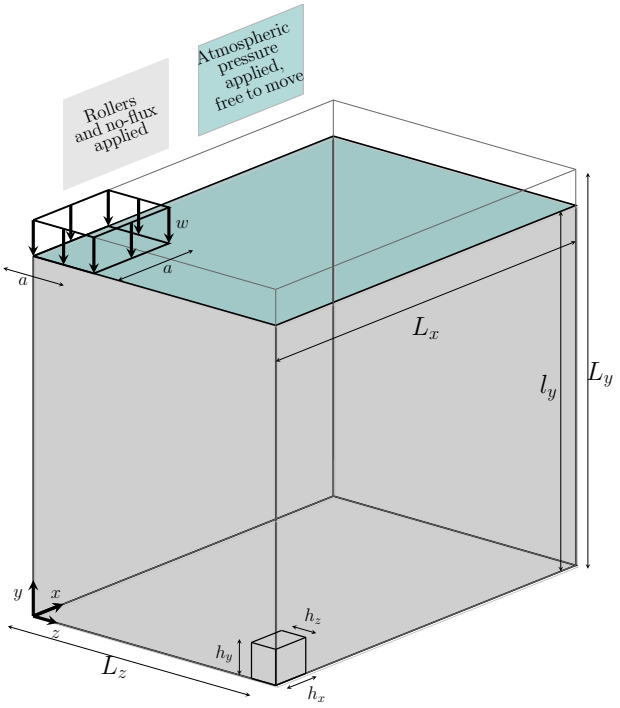

Figure 7: Initial setup for the 3D flexible footing problem.

rollers and no-flux conditions applied, except for the top surface, which is free to move and with zero atmospheric pressure applied. The simulations are run considering quasi-static conditions, where the overburden w linearly ramps from zero to a value of $5 \cdot 10^5$ Pa during 10 pseudo time-steps, while gravity effects are neglected. Eight material points per cell initially populate each mesh element.

Four simulations have been run: two analyses consider the elastic part described by the original linear Hencky material, while the other two take the improved Hencky material defined by Eq. (33) into account. All of the shared parameters of the simulations are listed in Table 2. Different initial values of the Eulerian porosity and bulk modulus (or its tangent value) are enumerated in Table 3. The reason why initial values of these parameters are considered lies in the direct implication of the Eulerian porosity and the bulk modulus on the volumetric behaviour. Moreover, as reported in Table 2, the hydraulic conductivity value is relatively low to make the overburden quickly balanced by the effective stress. The parameters relative to the $\alpha - \gamma$ model are taken from Coombs and Crouch [70].

As can be seen from Figure 8, all analyses considering the original Hencky material fail within the 10^{th} pseudo time-step, regardless of their initial value of Eulerian porosity or bulk modulus. Moreover, Figure 8 emphasises a strict correlation between negative values of the Eulerian porosity and failure of the analyses, with this latter phenomenon occurring a few time-steps after the former. The failure of the algorithm for this more complex situation adds confidence to the explanation provided for Example 4.2; that extremely simplistic situation represents a particular case in which the iterative method can find a solution even in adverse conditions. The improved Hencky material, conversely, permits all the considered simulations to be completed.

Contours of the Eulerian porosity plotted in Figure 9 show where the negative values of the original Hencky material occur, i.e., in the proximity of the applied load. Excluding a load disturbance zone (corresponding to the upper rows of material points), the zone below the foundation is the area where, as expected, inequality (30a) is violated by the original Hencky material.

Table 3: Summary of the different parameters considered in the analyses of the elasto-plastic flexible footing under large deformations.

	Case (A)	Case (B)
$K_0^{e,tan}$ / $\bar{K}$ [Pa]	$30 \cdot 10^6$	$50 \cdot 10^6$
n_0	0.2	0.1

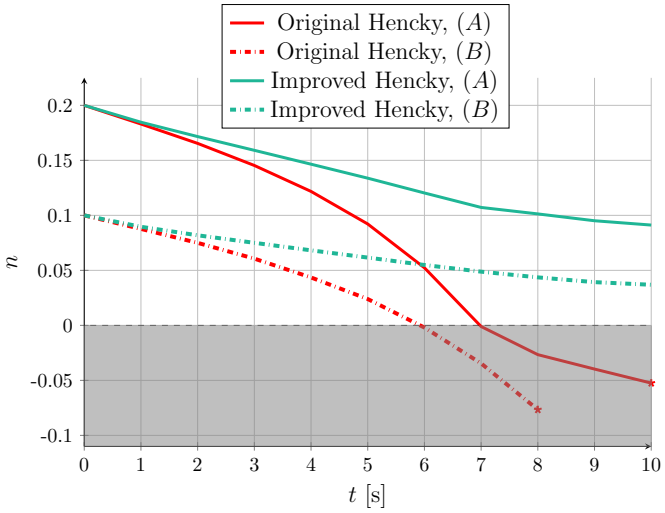

Figure 8: Time-plot of the porosity computed at the material point initially located at $(0.125, 9.625, 0.125)$ m for all of the simulations.

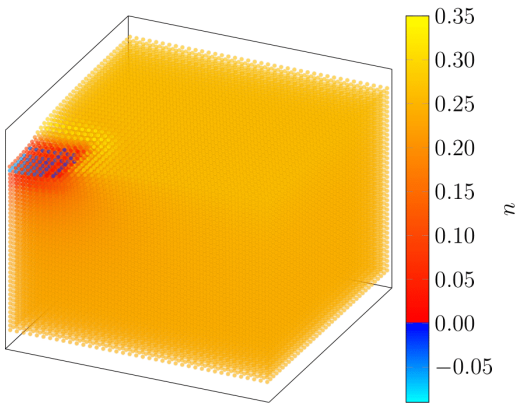

(a) Original Hencky, Analysis (A).

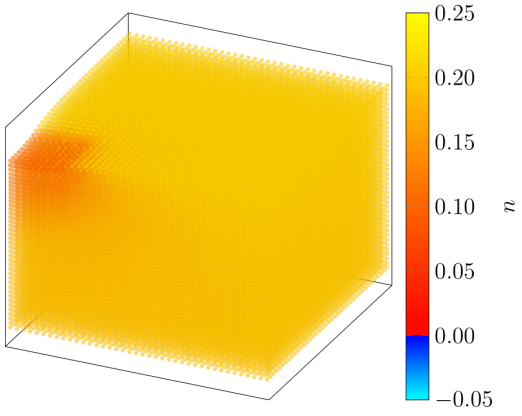

(b) Improved Hencky, Analysis (A).

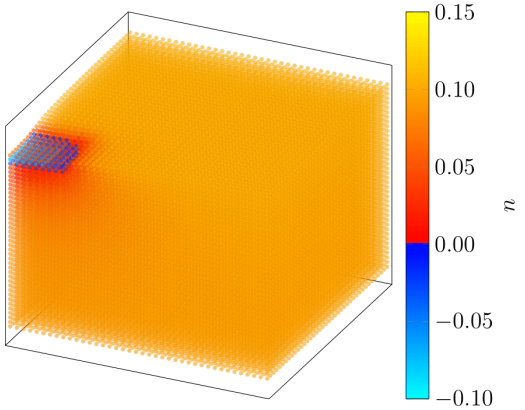

(c) Original Hencky, Analysis (B).

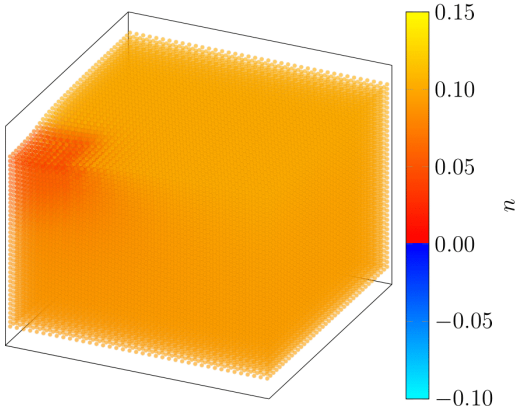

(d) Improved Hencky, Analysis (B).

Figure 9: Contours of the Eulerian porosity values applied to the final deflection shapes of the flexible footing problem.

5. Conclusion and future perspectives

This work emphasised that assuming Terzaghi effective stress decomposition comes with a specific cost in the context of finite strain mechanics. This particularly attractive stress decomposition, which stems from the assumption of solid matrix incompressibility, imposes a kinematic constraint on the material behaviour, this being $\epsilon_v \geq \ln(1 - n_0)$, implying the material becomes progressively incompressible when fluid mass is gradually expelled. When this constraint is not respected, negative values of the Eulerian are predicted, which are indicative of the violation of solid mass conservation. For those analyses not respecting such constraint, not only are the results questionable, but, as proven via Examples 4.2 and 4.3, this makes simulations highly unstable.

A way to respect this kinematic constraint has been proposed, modifying the free energy function of a classical Hencky material. This was achieved by considering a material whose volumetric behaviour depends on the Eulerian porosity. Modifying the stress-strain relationship has the advantage of strongly (point-wisely) introducing solid mass conservation. It was also demonstrated how this method can be incorporated into thermodynamically consistent treatments for elasticity (hyper-elasticity) and elasto-plasticity (hyper-plasticity), making it further appealing also for cyclic loading/displacements conditions. Owing to the setting of the new material into the elasto-plastic regime, the range of applicability of the improved Hencky material can span wildly, with intriguing applications in geomechanics (seismic or wind/wave loads applied to structures) to biomechanics (titanium implants in the human body).

Moreover, making the material's bulk modulus depending on the Eulerian porosity permits extending the kinematic constraint to all materials showing an additive decomposition between volumetric and deviatoric behaviour. For those materials which do not offer this decomposition, the constraint should be enforced through other methods, such as the penalty method or the Lagrange multiplier. However, this type of techniques implements the constraint weakly (in an integral sense) and, in addition, requires adding terms to the

weak form.

It must be noticed that the further the strains are from the incompressible limit, the more the modified Hencky material is similar to its original form. In other words, the improvement introduced to the Hencky material does not alter the type of material when it is far from that limit but, as the examples show, plays a crucial role in the proximity of that constraint.

Natural extensions of this model could evaluate the inclusion of the porosity-dependent volumetric behaviour in anisotropic media or understand the implications stemming from this assumption (i.e., porosity-dependent bulk modulus) when considering visco-elasto-plastic porous materials.

Acknowledgements

This research was supported by the UKRI Engineering and Physical Sciences Research Council (EPSRC) [grant number EP/R004900/1]. All data created during this research are openly available at collections.durham.ac.uk/ (specific DOI to be confirmed if/when the paper is accepted). The first author thanks Mr Luis Carlos Díaz for the productive debate, which dramatically improved the current work. The research presented in this article has also benefited from discussions with, and feedback from Robert Bird, Nathan Gavin, Ted O'Hare, Bradley Sims, Sam Sutcliffe and Jiayi Yuan. For the purpose of open access, the author has applied a Creative Commons Attribution (CC BY) licence to any Author Accepted Manuscript version arising.

Appendix A. Notes on the implementation of the modified Hencky model

As this appendix focuses more on the implementation, the *Voigt* notation, exploiting the symmetry of (both) $\boldsymbol{\tau}$ and $\boldsymbol{\epsilon}$, is used.

Before moving to the computation of the non-linear stress-strain relationship, it can be

convenient to compute the following derivatives

$$\frac{\partial \epsilon_v}{\partial \boldsymbol{\epsilon}} = \boldsymbol{I}^{(2)}; \tag{A.1}$$

$$\frac{\partial \epsilon_q}{\partial \boldsymbol{\epsilon}} = \frac{2}{3\,\epsilon_q}\bar{\boldsymbol{e}}; \tag{A.2}$$

$$\frac{\partial n}{\partial \epsilon_v} = \frac{1-n_0}{\exp\left(\epsilon_v\right)} = 1-n, \tag{A.3}$$

with the quantity $\bar{\boldsymbol{e}}$ being

$$\bar{\boldsymbol{e}} = \begin{bmatrix} e_{xx},\ e_{yy},\ e_{zz},\ 2\,e_{xy},\ 2\,e_{xz},\ 2\,e_{yz} \end{bmatrix}^T. \tag{A.4}$$

Appendix A.1. The elastic case

The step-by-step derivation of the Kirchhoff effective stress given by Eq. (34) is as follows

$$\begin{aligned} \boldsymbol{\tau}' =& \frac{\partial \hat{\Psi}^{sk}_{inc}}{\partial \boldsymbol{\epsilon}^e} = \frac{K}{2}\frac{\partial}{\partial \epsilon^e_v}\left(\frac{\left(\epsilon^e_v\right)^2}{n}\right)\boldsymbol{I}^{(2)} + \frac{3}{2}G\,\frac{\partial}{\partial \epsilon^e_q}\left(\left(\epsilon^e_q\right)^2\right)\frac{2}{3\,\epsilon^e_q}\bar{\boldsymbol{e}} = \\ =& \frac{K\,\epsilon^e_v}{n}\left(1+\frac{\epsilon^e_v}{2\,n}\left(n-1\right)\right)\boldsymbol{I}^{(2)} + 2G\,\bar{\boldsymbol{e}^e}, \end{aligned} \tag{A.5}$$

where derivatives (A.1)- (A.4) are particularised to the elastic case. As the value of the Eulerian porosity n is computed based on the Jacobian J via Eq. (23), it can be seen that the calculation of the effective stress (A.5) is straightforward once the decomposition of the elastic strain into a volumetric and a deviatoric part is performed.

The step-by-step linearisation of the effective stress-strain matrix given by Eq. (35) is

$$\begin{aligned} \boldsymbol{\mathcal{D}}^e \coloneqq& \frac{\partial^2 \hat{\Psi}^{sk}_{inc}}{\partial \boldsymbol{\epsilon}^e \otimes \partial \boldsymbol{\epsilon}^e} = \frac{\partial \boldsymbol{\tau}'}{\partial \boldsymbol{\epsilon}^e} = \\ =& \frac{\partial}{\partial \epsilon^e_v}\left(\frac{K\,\epsilon^e_v}{n}\left(1+\frac{\epsilon^e_v}{2\,n}\left(n-1\right)\right)\right)\boldsymbol{I}^{(2)}\otimes\boldsymbol{I}^{(2)} + 2\,G\,\frac{\partial \bar{\boldsymbol{e}}^e}{\partial \boldsymbol{\epsilon}^e} = \\ =& K^{e,\,tan}\,\boldsymbol{I}^{(2)}\otimes\boldsymbol{I}^{(2)} + 2\,G\,\boldsymbol{I}^{(4),\,dev}, \end{aligned} \tag{A.6}$$

where the full expression of $\boldsymbol{I}^{(4),\,dev}$ in Voigt notation is

$$\bar{\boldsymbol{I}}^{(4),\,dev} \coloneqq \begin{bmatrix} 2/3 & -1/3 & -1/3 & 0 & 0 & 0 \\ -1/3 & 2/3 & -1/3 & 0 & 0 & 0 \\ -1/3 & -1/3 & 2/3 & 0 & 0 & 0 \\ 0 & 0 & 0 & 2 & 0 & 0 \\ 0 & 0 & 0 & 0 & 2 & 0 \\ 0 & 0 & 0 & 0 & 0 & 2 \end{bmatrix}. \tag{A.7}$$

Appendix A.2. Elasto-plastic subroutine

This section details the computation of the effective stress in correspondence of elasto-plastic strains, as well as the computation of the consistent tangent matrix $\boldsymbol{\mathcal{D}}^{alg} \coloneqq \frac{\partial \boldsymbol{\tau}'}{\partial \boldsymbol{\epsilon}^{e,\,tr}}$ to provide optimal convergence of Newton's global process for implicit solvers is also outlined.

For this purpose, System (49) can be expressed as a linear form as

$$\begin{bmatrix} \boldsymbol{I}^{4,\,sym} + \Delta\gamma \frac{\partial^2 g}{\partial \boldsymbol{\tau}' \otimes \partial \boldsymbol{\tau}'} : \boldsymbol{\mathfrak{Y}} : \boldsymbol{\mathcal{D}}^e, & \left(\boldsymbol{I}^{4,\,sym} + \Delta\gamma \frac{\partial^2 g}{\partial \boldsymbol{\tau}' \otimes \partial \boldsymbol{\tau}'} : \boldsymbol{\mathfrak{Y}} : \boldsymbol{\mathcal{D}}^p \right) : \frac{\partial g}{\partial \boldsymbol{\tau}'} \\ \frac{\partial \Phi^{\tau'}}{\partial \boldsymbol{\tau}'} : \boldsymbol{\mathfrak{Y}} : \boldsymbol{\mathcal{D}}^e, & \frac{\partial \Phi^{\tau'}}{\partial \boldsymbol{\tau}'} : \boldsymbol{\mathfrak{Y}} : \boldsymbol{\mathcal{D}}^p : \frac{\partial g}{\partial \boldsymbol{\tau}'} \end{bmatrix} \begin{bmatrix} d\boldsymbol{\epsilon}^e \\ d\Delta\gamma \end{bmatrix} = \begin{bmatrix} d\boldsymbol{\epsilon}^{e,tr} \\ 0 \end{bmatrix}. \tag{A.8}$$

Eq. (A.8) can be rewritten with $d\boldsymbol{\tau}'$ being the unknown in lieu of $d\boldsymbol{\epsilon}^e$ via Eq. (48), resulting in

$$\begin{bmatrix} (\boldsymbol{\mathcal{D}}^e)^{-1} : \boldsymbol{\mathfrak{Y}}^{-1} + \Delta\gamma \frac{\partial^2 g}{\partial \boldsymbol{\tau}' \otimes \partial \boldsymbol{\tau}'}, & \left(\boldsymbol{I}^{4,\,sym} - (\boldsymbol{\mathcal{D}}^e)^{-1} : \boldsymbol{\mathcal{D}}^p \right) : \frac{\partial g}{\partial \boldsymbol{\tau}'} \\ \frac{\partial \Phi^{\tau'}}{\partial \boldsymbol{\tau}'} & 0 \end{bmatrix} \begin{bmatrix} d\boldsymbol{\tau}' \\ d\Delta\gamma \end{bmatrix} = \begin{bmatrix} d\boldsymbol{\epsilon}^{e,tr} \\ 0 \end{bmatrix}. \tag{A.9}$$

The inversion of (A.9) leads to

$$\begin{bmatrix} d\boldsymbol{\tau}' \\ d\Delta\gamma \end{bmatrix} = \begin{bmatrix} \mathbf{D}_{11} & \mathbf{D}_{12} \\ \mathbf{D}_{21} & \mathbf{D}_{22} \end{bmatrix} \begin{bmatrix} d\boldsymbol{\epsilon}^{e,tr} \\ 0 \end{bmatrix}, \tag{A.10}$$

where $\boldsymbol{\mathcal{D}}^{alg} = \frac{d\boldsymbol{\tau}'}{d\boldsymbol{\epsilon}^{e,tr}} = \mathbf{D}_{11}$.

Appendix B. Notes on hyper-plasticity

Appendix B.1 expands hyper-plasticity within the context of finite strain mechanics (firstly proposed by Oliynyk and Tamagnini [71]) to isotropic coupled materials. Appendix B.2 shows how to compute the yield function and the flow rule used in Example 4.3 for the improved Hencky material and the dissipation function proposed by Collins and Hilder [43].

Owing to the use of unsymmetrical tensors, this section makes use of Einstein index notation for repeated indices.

Appendix B.1. Hyper-plastic formulation in finite strain

Clausius-Planck inequality (29) provides the basis for hyper-plastic formulations. This can be written in a more compact form as follows

$$\tau'_{ij}\, d_{ij} = J\, \mathcal{D}^{sk} + \dot{\hat{\Psi}}^{sk}_{inc}. \tag{B.1}$$

Let us, without any loss of generality, consider the case where the free energy function Eq. (33) do not include further hardening, i.e., $\tilde{\Psi}^{sk}_{inc}(\boldsymbol{\alpha}) = 0$. In this case, the isotropic free energy function is a function of the left Cauchy-Green strain tensor, i.e., $\hat{\Psi}^{sk}_{inc}(\boldsymbol{b}^e, \boldsymbol{b}^p)$,

which implies

$$\dot{\hat{\Psi}}^{sk}_{inc}\left(\boldsymbol{b}^e,\boldsymbol{b}^p\right)=\frac{\partial\hat{\Psi}^{sk}_{inc}}{\partial b^e_{ij}}\dot{b}^e_{ij}+\frac{\partial\hat{\Psi}^{sk}_{inc}}{\partial b^p_{ij}}\dot{b}^p_{ij}=2\frac{\partial\hat{\Psi}^{sk}_{inc}}{\partial b^e_{ij}}\underbrace{b^e_{jk}\,d^e_{ki}}_{=\dot{b}^e_{ij}}+2\frac{\partial\hat{\Psi}^{sk}_{inc}}{\partial b^p_{ij}}\underbrace{b^p_{jk}\left(F^e\right)^{-1}_{il}d^p_{lm}\,F^e_{mk}}_{=\dot{b}^p_{ij}},\quad\text{(B.2)}$$

where the right-hand side of the above equation uses the kinematic relationships $\dot{\boldsymbol{b}}^p=\bar{\boldsymbol{L}}^p\boldsymbol{b}^p+\boldsymbol{b}^p\left(\bar{\boldsymbol{L}}^p\right)^T$, with $\bar{\boldsymbol{L}}^p\coloneqq\dot{\boldsymbol{F}}^p\left(\boldsymbol{F}^p\right)^{-1}$ and $\boldsymbol{l}^p\coloneqq\boldsymbol{F}^e\bar{\boldsymbol{L}}^p\left(\boldsymbol{F}^e\right)^{-1}$.

Eq. (31a) gives what is referred to as the *true stresses* in the context of hyper-plasticity, which, in this work, matches the definition of effective stresses. Two other kinds of stresses are usually provided in the context of hyper-plasticity, these being the *shift stress* and the *dissipative stress*, defined as

$$\chi'_{lm}\coloneqq 2\frac{\partial\hat{\Psi}^{sk}_{inc}}{\partial b^p_{ij}}b^p_{jk}\left(F^e\right)^{-1}_{il}\,F^e_{mk};\quad\text{(B.3)}$$

$$\varphi'_{ij}\coloneqq\frac{\partial\left(J\,\mathcal{D}^{sk}\right)}{\partial d^p_{ij}}.\quad\text{(B.4)}$$

Owing to the simplification $\tilde{\Psi}^{sk}_{inc}(\boldsymbol{\alpha})=0$, inequality (31b) suggests the dissipation $J\,\mathcal{D}^{sk}$ to be dependent only from the plastic stretching tensor $\boldsymbol{d}^p$. Having also excluded the viscosity effects (i.e., the material is rate-indipendent), it is possible to postulate (see, in this regards, Oliynyk and Tamagnini [71]) that the dissipation is homogenous of degree one in the plastic stretching tensor. According to Euler's theorem for homogeneous functions, it then follows

$$J\,\mathcal{D}^{sk}=\frac{\partial\left(J\,\mathcal{D}^{sk}\right)}{\partial d^p_{ij}}d^p_{ij}=\varphi'_{ij}\,d^p_{ij},\quad\text{(B.5)}$$

where definition (B.4) has been used on the right-hand side of the above equation.

Owing to Eqs. (B.2)-(B.5), Eq. (B.1) becomes

$$\tau'_{ij}\,d_{ij}=\varphi'_{ij}\,d^p_{ij}+\tau'_{ij}\,d^e_{ij}+\chi'_{ij}\,d^p_{ij},\quad\text{(B.6)}$$

which provides the following relationship among stresses

$$\tau'_{ij} = \varphi'_{ij} + \chi'_{ij}. \tag{B.7}$$

Appendix B.2. Yield function and flow rule

Considering the free energy function given by Eq. (33), the shift stress can be written

$$\chi'_{lm} = 2\frac{\partial \hat{\Psi}^{sk}_{inc}}{\partial b^p_{ij}} b^p_{jk} \left(F^e\right)^{-1}_{il} F^e_{mk} = \frac{\partial \hat{\Psi}^{sk}_{inc}}{\partial \epsilon^p_v} \delta_{ik} \left(F^e\right)^{-1}_{il} F^e_{mk} = \underbrace{\frac{K}{2n^2}\left(\epsilon^e_v\right)^2 (n-1)}_{:=p^{\chi'}} \delta_{lm}, \tag{B.8}$$

while the effective stress has been already given by (A.5).

To compute the dissipative stress and provide a thermodynamically consistent yield function and flow rule, it is necessary to introduce a particular function for the dissipation $J\mathcal{D}^{(sk)}$. This work takes the $\alpha - \gamma$ family of models proposed by Collins and Hilder [43] into account and adapts it to the case of finite strain. For these models, the dissipation function is given by

$$J\,\mathcal{D}^{sk} = \sqrt{\left(d^p_v\, A\right)^2 + \left(d^p_\gamma\, B\right)^2} \geq 0, \tag{B.9}$$

where $d_v \coloneqq d_{ij}\delta_{ij}$ and $d_\gamma \coloneqq \sqrt{\left(d_{ij} - \frac{d_v}{3}\delta_{ij}\right) : \left(d_{ij} - \frac{d_v}{3}\delta_{ij}\right)}$. Eq. (B.9) introduces also two pressure-dependent parameters A and B, these being

$$A \coloneqq (1-\gamma)\, p' + \frac{\gamma}{2} p_c \qquad B \coloneqq M\left((1-\alpha)\, p' + \alpha \frac{\gamma}{2} p_c\right). \tag{B.10}$$

As further hardening has been excluded, p_c is considered as constant in this work, but, generally speaking, it can vary (see Coombs and Crouch [70] in this regard).

Eq. (B.9) permits calculating the dissipative stresses for this particular case of the

dissipation function, these being

$$\varphi'_{ij} = \frac{\partial \left(J\, D^{sk} \right)}{\partial d^p_{ij}} = \underbrace{\frac{\partial \left(J\, D^{sk} \right)}{\partial d^p_v}}_{:= p^{\varphi'}} \delta_{ij} + \underbrace{\frac{\partial \left(J\, D^{sk} \right)}{\partial d^p_\gamma}}_{:= q^{\varphi'}} \frac{\partial d^p_\gamma}{\partial d^p_{ij}}, \tag{B.11}$$

where, for the general symmetric stress tensor $(\bullet)_{ij}$, $p^{(\bullet)} := \frac{1}{3} (\bullet)_{ij}\ \delta_{ij}$, $s^{(\bullet)}_{ij} := (\bullet)_{ij} - p^{(\bullet)} \delta_{ij}$, and $q^{(\bullet)} := \sqrt{s^{(\bullet)}_{ij}\ s^{(\bullet)}_{ij}}$. The one-to-one correspondence between power-conjugates allows to express the dissipative stress invariants as follows

$$p^{\varphi'} = \frac{A^2 d^p_v}{J\, D^{sk}}; \tag{B.12}$$

$$q^{\varphi'} = \frac{B^2 d^p_\gamma}{J\, D^{sk}}, \tag{B.13}$$

or, inverting these relationships,

$$d^p_v = \frac{p^{\varphi'} J\, D^{sk}}{A^2}; \tag{B.14}$$

$$d^p_\gamma = \frac{q^{\varphi'} J\, D^{sk}}{B^2}. \tag{B.15}$$

Substituting the above expression for stretching invariants in Eq. (B.9) and eliminating the dissipation results in

$$1 = \left(\frac{p^{\varphi'}}{A} \right)^2 + \left(\frac{q^{\varphi'}}{B} \right)^2, \tag{B.16}$$

which, moving all of the components on one side of the equation, gives the *dissipative yield condition*

$$\Phi^{\varphi'} = \left(B p^{\varphi'} \right)^2 + \left(A q^{\varphi'} \right)^2 - A^2 B^2 = 0. \tag{B.17}$$

Shifting the above condition to the effective stress space (i.e., using Eq. (B.7)) is necessary

to compute the *yield function*, this being

$$\Phi^{\tau'} = B^2 \left(p' - p^{\chi'}\right)^2 + \left(Aq^{\tau'}\right)^2 - A^2B^2 = 0 \tag{B.18}$$

As required for coupled materials (see Collins and Houslby [41] and Collins [58]) the direction of the flow rule is given by the normal to dissipative yield function in the dissipative stress space, i.e.,

$$\frac{\partial \Phi^{\varphi'}}{\partial \varphi'_{ij}} = -2B^2 p^{\varphi'} \frac{1}{3} \delta_{ij} + 2A^2 s_{ij}^{\varphi'}, \tag{B.19}$$

where the sign of pressure have been changed from the geotechnical convention (where compression is considered positive) to that more commonly used in mechanics and adopted throughout this work. The direction of the plastic flow is given by shifting the above equation in the true stress spaces, this being

$$\frac{\partial g}{\partial \tau'_{ij}} = -2B^2 \left(p' - p^{\chi'}\right) \frac{1}{3} \delta_{ij} + 2A^2 s_{ij}. \tag{B.20}$$

References

[1] N. Castelletto, G. Gambolati, P. Teatini, A coupled mfe poromechanical model of a large-scale load experiment at the coastland of venice, Computational Geosciences 19 (2015) 17–29.

[2] A. Karrech, M. Attar, M. Elchalakani, H. Basarir, F. Abbassi, A. Seibi, The poromechanics of massive fluid injection in natural environments, in: ISRM 1st International Conference on Advances in Rock Mechanics-TuniRock 2018, OnePetro, 2018, pp. 17–22.

[3] M. Hettema, P. Schutjens, B. Verboom, H. Gussinklo, Production-induced compaction of a sandstone reservoir: the strong influence of stress path, SPE Reservoir Evaluation & Engineering 3 (04) (2000) 342–347.

[4] A. Karrech, T. Poulet, K. Regenauer-Lieb, Poromechanics of saturated media based on the logarithmic finite strain, Mechanics of Materials 51 (2012) 118–136.

[5] O. C. Zienkiewicz, A. Chan, M. Pastor, B. Schrefler, T. Shiomi, Computational geomechanics, Vol. 613, Citeseer, 1999.

[6] S. C. Cowin, Bone poroelasticity, Journal of biomechanics 32 (3) (1999) 217–238.

[7] M. A. Biot, General theory of three-dimensional consolidation, Journal of applied physics 12 (2) (1941) 155–164.

[8] M. A. Biot, Theory of propagation of elastic waves in a fluid-saturated porous solid. ii. higher frequency range, The Journal of the acoustical Society of america 28 (2) (1956) 179–191.

[9] M. A. Biot, Mechanics of deformation and acoustic propagation in porous media, Journal of applied physics 33 (4) (1962) 1482–1498.

[10] R. De Boer, W. Ehlers, A historical review of the formulation of porous media theories, Acta Mechanica 74 (1-4) (1988) 1–8.

[11] C. W. MacMinn, E. R. Dufresne, J. S. Wettlaufer, Large deformations of a soft porous material, Physical Review Applied 5 (4) (2016) 044020.

[12] A. Selvadurai, A. Suvorov, Coupled hydro-mechanical effects in a poro-hyperelastic material, Journal of the Mechanics and Physics of Solids 91 (2016) 311–333.

[13] Y. Zhang, Mechanics of adsorption–deformation coupling in porous media, Journal of the Mechanics and Physics of Solids 114 (2018) 31–54.

[14] B. Nedjar, Formulation of a nonlinear porosity law for fully saturated porous media at finite strains, Journal of the Mechanics and Physics of Solids 61 (2) (2013) 537–556.

[15] B. Nedjar, On finite strain poroplasticity with reversible and irreversible porosity laws. formulation and computational aspects, Mechanics of Materials 68 (2014) 237–252.

[16] L. S. Bennethum, Compressibility moduli for porous materials incorporating volume fraction, Journal of engineering mechanics 132 (11) (2006) 1205–1214.

[17] D. Bernaud, V. Deudé, L. Dormieux, S. Maghous, D. Schmitt, Evolution of elastic properties in finite poroplasticity and finite element analysis, International Journal for Numerical and Analytical Methods in Geomechanics 26 (9) (2002) 845–871.

[18] H. Hencky, The elastic behavior of vulcanized rubber, Journal of Applied Mechanics (1933).

[19] O. Coussy, Poromechanics, John Wiley & Sons, 2004.

[20] R. Lewis, B. Schrefler, The Finite Element Method in the Static and Dynamic Deformation and Consolidation of Porous Media, John Wiley & Sons, New York, 1998.

[21] E. Kröner, Allgemeine kontinuumstheorie der versetzungen und eigenspannungen, Archive for Rational Mechanics and Analysis 4 (1) (1959) 273–334.

[22] E. H. Lee, Elastic-plastic deformation at finite strains, Journal of Applied Mechanics 36 (1) (1969) 1–6.

[23] J. Mandel, Plasticité Classique et Viscoplasticité, Vol. 97 of CISM Courses and Lectures, Springer, 1971.

[24] K. Bennett, R. Regueiro, R. Borja, Finite strain elastoplasticity considering the eshelby stress for materials undergoing plastic volume change, International Journal of Plasticity 77 (2016) 214–245.

[25] E. A. de Souza Neto, D. Peric, D. R. Owen, Computational methods for plasticity: theory and applications, John Wiley & Sons, 2011.

[26] W. Sun, J. T. Ostien, A. G. Salinger, A stabilized assumed deformation gradient finite element formulation for strongly coupled poromechanical simulations at finite strain, International Journal for Numerical and Analytical Methods in Geomechanics 37 (16) (2013) 2755–2788.

[27] R. M. Bowen, Compressible porous media models by use of the theory of mixtures, International Journal of Engineering Science 20 (6) (1982) 697–735.

[28] F. Armero, Formulation and finite element implementation of a multiplicative model of coupled poro-plasticity at finite strains under fully saturated conditions, Computer methods in applied mechanics and engineering 171 (3-4) (1999) 205–241.

[29] A. Gajo, A general approach to isothermal hyperelastic modelling of saturated porous media at finite strains with compressible solid constituents, Proceedings of the Royal Society A: Mathematical, Physical and Engineering Sciences 466 (2122) (2010) 3061–3087.

[30] J. C. Simo, Numerical analysis and simulation of plasticity, Handbook of numerical analysis 6 (1998) 183–499.

[31] L. Anand, A large deformation poroplasticity theory for microporous polymeric materials, Journal of the Mechanics and Physics of Solids 98 (2017) 126–155.

[32] A. Gajo, Finite strain hyperelastoplastic modelling of saturated porous media with compressible constituents, International journal of solids and structures 48 (11-12) (2011) 1738–1753.

[33] B. Coleman, W. Noll, The thermodynamics of elastic materials with heat conduction, Arch. Ration. Mech. Anal 13 (1963) 167.

[34] B. D. Coleman, M. E. Gurtin, Thermodynamics with internal state variables, The journal of chemical physics 47 (2) (1967) 597–613.

[35] L. Morland, A simple constitutive theory for a fluid-saturated porous solid, Journal of geophysical research 77 (5) (1972) 890–900.

[36] O. Coussy, Thermomechanics of saturated porous solids in finite deformation, European journal of mechanics. A. Solids 8 (1) (1989) 1–14.

[37] S. Advani, T. Lee, J. Lee, C. Kim, Hygrothermomechanical evaluation of porous media under finite deformation. part i-finite element formulations, International journal for numerical methods in engineering 36 (1) (1993) 147–160.

[38] J. Bluhm, Zur berucksichtigung der kompressibilitat des festkorpers bei porosen materialien, ZAMM-Zeitschrift fur Angewandte Mathematik und Mechanik 77 (1) (1997) S39.

[39] K. Terzaghi, Theoretical soil mechanics. usa: John and wiley and sons (1943).

[40] R. I. Borja, E. Alarcón, A mathematical framework for finite strain elastoplastic consolidation part 1: Balance laws, variational formulation, and linearization, Computer Methods in Applied Mechanics and Engineering 122 (1-2) (1995) 145–171.

[41] I. Collins, G. Houlsby, Application of thermomechanical principles to the modelling of geotechnical materials, Proceedings of the Royal Society of London. Series A: Mathematical, Physical and Engineering Sciences 453 (1964) (1997) 1975–2001.

[42] I. Collins, P. Kelly, A thermomechanical analysis of a family of soil models, Géotechnique 52 (7) (2002) 507–518.

[43] I. F. Collins, T. Hilder, A theoretical framework for constructing elastic/plastic constitutive models of triaxial tests, International journal for numerical and analytical methods in geomechanics 26 (13) (2002) 1313–1347.

[44] I. Collins, A systematic procedure for constructing critical state models in three dimensions, International Journal of Solids and Structures 40 (17) (2003) 4379–4397.

[45] I. Collins, B. Muhunthan, On the relationship between stress–dilatancy, anisotropy, and plastic dissipation for granular materials, Geotechnique 53 (7) (2003) 611–618.

[46] I. F. Collins, Elastic/plastic models for soils and sands, International Journal of Mechanical Sciences 47 (4-5) (2005) 493–508.

[47] I. Collins, The concept of stored plastic work or frozen elastic energy in soil mechanics, Geotechnique 55 (5) (2005) 373–382.

[48] I. Collins, B. Muhunthan, A. Tai, M. Pender, The concept of a 'reynolds–taylor state'and the mechanics of sands, Geotechnique 57 (5) (2007) 437–447.

[49] I. Collins, B. Muhunthan, B. Qu, Thermomechanical state parameter models for sands, Géotechnique 60 (8) (2010) 611–622.

[50] P. Flory, Thermodynamic relations for high elastic materials, Transactions of the Faraday Society 57 (1961) 829–838.

[51] K. N. Nordstrom, E. Verneuil, W. G. Ellenbroek, T. C. Lubensky, J. P. Gollub, D. J. Durian, Centrifugal compression of soft particle packings: Theory and experiment, Physical Review E 82 (4) (2010) 041403.

[52] D. R. Hewitt, J. S. Nijjer, M. G. Worster, J. A. Neufeld, Flow-induced compaction of a deformable porous medium, Physical Review E 93 (2) (2016) 023116.

[53] M. Zytynski, M. Randolph, R. Nova, C. Wroth, On modelling the unloading-reloading behaviour of soils, International Journal for Numerical and Analytical Methods in Geomechanics 2 (1) (1978) 87–93.

[54] J. C. Simo, Algorithms for static and dynamic multiplicative plasticity that preserve the classical return mapping schemes of the infinitesimal theory, Computer Methods in Applied Mechanics and Engineering 99 (1) (1992) 61–112.

[55] S. Reese, P. Wriggers, A material model for rubber-like polymers exhibiting plastic deformation: computational aspects and a comparison with experimental results, Computer methods in applied mechanics and engineering 148 (3-4) (1997) 279–298.

[56] S. Doll, K. Schweizerhof, On the development of volumetric strain energy functions, J. Appl. Mech. 67 (1) (2000) 17–21.

[57] J. Lubliner, On the thermodynamic foundations of non-linear solid mechanics, International Journal of Non-Linear Mechanics 7 (3) (1972) 237–254.

[58] I. Collins, Associated and non-associated aspects of the constitutive laws for coupled elastic/plastic materials, The International Journal Geomechanics 2 (2) (2002) 259–267.

[59] G. Houlsby, A. Puzrin, Principles of hyperplasticity: an approach to plasticity theory based on thermodynamic principles (1985).

[60] S. Murakami, Continuum damage mechanics: a continuum mechanics approach to the analysis of damage and fracture, Vol. 185, Springer Science & Business Media, 2012.

[61] Y. Yamakawa, Hyperelastic constitutive models for geomaterials: Extension of existing models to include finite strains and their comparison, Computers and Geotechnics 143 (2022) 104600.

[62] T. Charlton, W. Coombs, C. Augarde, igimp: An implicit generalised interpolation material point method for large deformations, Computers & Structures 190 (2017) 108–125.

[63] W. M. Coombs, C. E. Augarde, Ample: A material point learning environment, Advances in Engineering Software 139 (2020) 102748.

[64] K. Soga, E. Alonso, A. Yerro, K. Kumar, S. Bandara, Trends in large-deformation

analysis of landslide mass movements with particular emphasis on the material point method, Géotechnique 66 (3) (2016) 248–273.

[65] Y. Zhao, J. Choo, Stabilized material point methods for coupled large deformation and fluid flow in porous materials, Computer Methods in Applied Mechanics and Engineering 362 (2020) 112742.

[66] S. Bandara, K. Soga, Coupling of soil deformation and pore fluid flow using material point method, Computers and geotechnics 63 (2015) 199–214.

[67] E. Love, D. L. Sulsky, An unconditionally stable, energy–momentum consistent implementation of the material-point method, Computer methods in applied mechanics and engineering 195 (33-36) (2006) 3903–3925.

[68] S. G. Bardenhagen, E. M. Kober, The generalized interpolation material point method, Computer Modeling in Engineering and Sciences 5 (6) (2004) 477–496.

[69] D. Boffi, F. Brezzi, M. Fortin, et al., Mixed finite element methods and applications, Vol. 44, Springer, 2013.

[70] W. M. Coombs, R. S. Crouch, Algorithmic issues for three-invariant hyperplastic critical state models, Computer methods in applied mechanics and engineering 200 (25-28) (2011) 2297–2318.

[71] K. Oliynyk, C. Tamagnini, Finite deformation hyperplasticity theory for crushable, cemented granular materials, Open Geomechanics 2 (2020) 1–33.